Ultrasound tissue classification

Shan, Caifeng; Tan, Tao; Han, Jungong; Huang, Di

Published in:
Artificial Intelligence Review

Publication date:
2020

Citation for published version (APA):
Shan, C., Tan, T., Han, J., & Huang, D. (2020). Ultrasound tissue classification: A review. *Artificial Intelligence Review*.

Ultrasound Tissue Classification: A Review

Caifeng Shan, Tao Tan, Jungong Han, Di Huang

***Abstract*— Ultrasound (US) imaging is the most widespread medical imaging modality for creating images of the human body in clinical practice. Tissue classification in ultrasound has been established as one of the most active research areas, driven by many important clinical applications. In this paper, we present a survey on ultrasound tissue classification, focusing on recent advances in this area. We start with a brief review on the main clinical applications. We then introduce the traditional approaches, where the existing research on feature extraction and classifier design are reviewed. As deep learning approaches becoming popular for medical image analysis, the recent deep learning methods for tissue classification are also introduced. We briefly discuss the FDA-cleared techniques being used clinically. We conclude with the discussion on the challenges and research focus in future.**

***Index Terms*— Tissue Classification, Tissue Characterization, Machine Learning, Deep Learning, Ultrasound Image Analysis**

I. Introduction

Different medical imaging modalities are available and widely used nowadays in clinical practice to create images of the human body, such as computed tomography (CT), magnetic resonance imaging (MR), positron emission tomography (PET), and ultrasound (US). Among those, US imaging is the most widespread modality for visualizing human soft tissue, because of its advantages compared to others: cheap, harmless (no ionizing radiations), allowing real-time feedback, convenient to operate, well established technology present in all places, and so on. On the other hand, because of the limited field of view, shadows, speckle noise, and other artifacts in the US images, the interpretation of US images is sometimes difficult.

One main target of US image (signal) analysis is tissue classification. Ultrasound tissue classification is to analyze the characteristics of the US data and their correlation to the pathological state of tissue, and design a classifier to distinguish the US data into different tissue types (or states). Tissue classification in ultrasound has many important applications, such as cancer diagnosis (in prostate, breast, liver, etc.) and cardiovascular disease diagnosis and intervention. Driven by the unmet clinical needs to distinguish different tissue types (e.g., healthy versus diseased) in US, tissue characterization and classification have received much attention in recent years [1], [2].

Traditionally the process of tissue classification can be divided into two main steps: 1) **feature extraction**: in this step, ultrasound modelling and signal analysis techniques are used to extract characteristic features from US image (signal) that can describe and hopefully differentiate different tissue types [1]. These characteristics may not be visible to human eyes, and it is necessary to examine the ultrasound image. If the features are discriminative, different tissue types will be represented as separate clusters in the feature space. Unfortunately in practice most extracted features have low discriminative power. Therefore, in order to discriminate different tissue types, a proper classifier is needed. This is step 2): **classifier design**, which aims to define the optimal decision boundary in the feature space to separate different tissue types. The classifier can be trained by applying machine learning and pattern recognition techniques on the data with ground truth. Different techniques have been exploited for ultrasound tissue classification.

Since 2012, **deep learning** algorithms such as convolutional neural networks (CNNs) [3] have become a powerful tool for automatically classifying pixels (patches) in the images. It usually contains several pairs of a convolution layer and a pooling layer. These layers behave as feature extractors. The intermediate outputs of these layers are fully connected to a multi-layer perception neural network for the classification task. New techniques including dropout [4], batch normalization [5] and resnetblock [6] were proposed to improve performance of neural networks. Deep learning approaches have been extensively exploited for medical image analysis, including tissue classification in ultrasound.

Ultrasound tissue classification is difficult, because the interaction between biological tissue (an inhomogeneous medium) and acoustic wave is very hard to model [1]. Although the quality of ultrasound images, in terms of signal-to-noise and contrast-to-noise ratios, has been improved substantially in recent years, it remains a challenging task to classify different tissue types in US images. This paper attempts to provide a review on ultrasound tissue classification, particularly focusing on recent advances in this area. The work on tissue characterization prior to 2009 was reviewed in the articles [1], [2].

The paper is organized as follows. We start with a brief review on the main clinical applications in Section II. We then introduce the existing research on feature extraction and classifier design in Section III and Section IV respectively. The recent deep learning approaches for tissue classification are discussed in Section V. Section VI introduces the FDA-cleared machine learning algorithms being used clinically. Section VII discusses the challenges and research directions in future, and finally Section VIII concludes the paper.

II. Clinical Applications

Medical ultrasound has a very broad range of clinical uses. Ultrasound tissue classification can be applied in many clinical fields, for instance, tissue classification plays an important role in ultrasound-based cancer diagnosis, e.g., by classifying the tissue regions as benign or malignant. Here we briefly introduce the main clinical applications that have received the most attention in the recent literature.

A. Cardiology

The primary aim of non-invasive cardiac imaging is to provide information on the diagnosis and severity of underlying cardiac conditions [7]. Echocardiography (ultrasound imaging of the heart) is the most common cardiac imaging procedure performed in clinical practice, due to its portability, low cost, and patient acceptance.

C. Shan is with College of Electrical Engineering and Automation, Shandong University of Science and Technology, Qingdao 266590, China

T. Tan is with Eindhoven University of Technology, Eindhoven 5600 MB, The Netherlands

J. Han is with Department of Computer Science, Aberystwyth University, SY23 3DB, UK

D. Huang is with Beijing Advanced Innovation Center for Big Data and Brain Computing, Beihang University, Beijing 100191, China

C. Shan (caifeng.shan@gmail.com) is the corresponding author.

Echocardiography has also been one of the driving application areas of medical ultrasound [8]. Cardiac imaging techniques characterise the underlying tissue directly, by assessing a signal from the tissue itself, or indirectly, by inferring tissue characteristics from global or regional function [7]. Although Cardiac Magnetic Resonance (CMR) imaging currently is the most investigated modality for tissue characterisation, this technology is difficult to scale up for routine use. On the other hand, echocardiography remains the primary imaging tool for most patients, so it represents an attractive alternative for cardiac tissue characterization.

Traditionally, integrated backscatter, which measures the ultrasonic reflectivity of the region of interest, was a major focus of tissue characterisation research [9]. However, backscatter has limited ability to reflect fibrosis in those with lower levels of myocardial fibrosis, such as coronary artery disease [10]. In [11], the frequency content from echocardiography and spectral analysis techniques were investigated for differentiating three different cardiac tissue types (cardiac adipose tissue, myocardium, and blood). Recently texture features of myocardium have been extracted from still ultrasound images for tissue characterization [12]. Speckle tracking echocardiography (STE) is a technique used to assess myocardial deformation at both segmental and global levels. Since distinct myocardial pathologies affect deformation differently, information about the underlying tissue can be inferred by STE. While other modalities such as CMR assess tissue characteristics through changes in the acquired myocardial tissue images, STE deformation parameters assess the impact of underlying pathology on tissue function. The available studies correlating STE deformation parameters with underlying tissue characteristics are reviewed in [7]. The most commonly used deformation measurements are those of strain (the change in length compared to initial length), strain rate (strain divided by time), and rotation (or twist). Machine learning and deep learning methods have been explored with STE features for tissue classification [13], [14].

In recent years ultrasound has been increasingly used for image-guided cardiac interventions or therapy [16]–[18]. Cardiac ablation, to create a set of transmural lesions in cardiac tissue, has been the main therapy method for atrial fibrillation. In thermal ablation, the target tissue is coagulated by transferring heat to the target area. Radio-frequency (RF) ablation and the lesion created by RF ablation are illustrated in Figure 1. One challenge for ablation therapy is the monitoring of the temperature rise and the extend of the ablated region in the tissue. US-based techniques for evaluating heat-induced lesions have been studied recently [15], [19], [20]. In an earlier work [21], both the textural and spectral features were considered for analyzing the ablated regions in the tissue. Methods have also been developed to estimate the temperature increase during the ablation process by detecting the change of sound speed, attenuation coefficient, and backscattering. In [19], US imaging is employed to investigate the temporal evolution and spatial extent of the lesion created by the HIFU (high intensity focused ultrasound) ablation. It is shown that spectral analysis of RF signals, which is related to the physical scatter properties, can potentially be used for monitoring the evolution of HIFU lesions. Imani *et al.* [20], [22] proposed to classify ablated tissue using RF time series features. The acoustical coefficient of nonlinearity is estimated in [23] for discriminating tissues during cardiac ablation therapy.

B. Vascular Disease

Cardiovascular diseases are responsible for a third of all deaths in women worldwide and more than a half in men [24]. Ultrasound imaging has become one of the most important modalities used in the assessment of vascular diseases. Virtually all peripheral arterial and venous structures can be visualized with the duplex ultrasound (DU), which currently is the main diagnostic modality used in deep venous thrombosis and carotid disease [25]. For carotid artery disease, the carotid plaque is traditionally judged according to the degree of stenosis and a 70% or greater diameter loss is an indication for surgery. Later it was recognized that not only must the degree of stenosis be evaluated, but also the carotid plaque instability, as it is an important determinant of stroke risk [26]. The DU allows for the study of plaque constituents; for instance, fibrotic tissue, which renders the plaque more stable, has different brightness from lipids. Traditionally the carotid plaque composition is determined based on the pixel brightness, i.e., using a threshold-based method. In [26], a multi-scale descriptor was used for pixel-level tissue classification in DU images. Similarly, various image features were considered in [27], [28] for plaque classification. A recent review on carotid artery ultrasound image analysis can be found in [29].

In the era of atherosclerosis, intravascular ultrasound (IVUS), a catheter-based imaging technique, has evolved as a valuable technique for diagnosis and intervention for coronary disease, by providing more precise measurement on intimal thickness and vulnerable plaques. In contrast, angiography, the traditionally used gold-standard in the imaging of vascular morphology, can only depict contrast agent filled lumen and not the vessel wall [25]. IVUS provides images of vascular structure by scanning inside the vessel, which are acquired by a mechanically rotated transducer or a multi-element transducer array. For the latter case, an array of transducers is disposed around the probe, with the synchronized emission of US waves. The imaging plane, perpendicular to the long axis of the catheter, provides a 360 degree image of the vessel. An example IVUS image is shown in Figure 2. By converting the A-lines from polar to cartesian coordinates, the full circumference of the vessel wall can be visualized. Therefore, all components of the vessel are visualized: the cross sectional luminal size, shape and vessel wall, as well as the various layers of the wall. IVUS has been used to guide the intervention by analyzing the vessel condition, e.g., assessing the atherosclerotic plaque amount and composition. IVUS can also be used to check the vessel condition after the intervention, and to monitor the status of disease over the time.

In IVUS images, calcifications are demonstrated as hyperechoic areas, whereas hemorrage or fat deposition inside an atheromatic plaque is hypoechoic. Subsequently, the plaque can be classified as lipid, calcified and fibrous, according to its acoustic properties [30] Tissue classification in IVUS images can automatically predict vulnerable plaques as well as quantify the amount of the different tissues; many approaches have been proposed in literature [31]–[36], which will be discussed in detail in the following sections.

C. Breast Cancer

Breast cancer is the most common cancer in women globally, and early detection is the key to reduce the death rate. Women with dense breasts have a risk of breast cancer four to six times higher than that of women with no or little dense tissue [37]. To improve cancer detection in dense breasts, personalized breast cancer screening with ultrasound has been proposed for women with dense breasts and women with elevated risk factors for developing breast cancer. Supplemental breast ultrasound (BUS) cancer screening can detect small, early stage invasive cancers that appear to be occult on mammograpms due to breast density [38]. Furthermore, BUS is more convenient and safer for clinical use [39] and it can be used as an alternative screening device to mammography for women with harmful mutations in either BRCA1 (breast cancer gene type1) or BRCA2 since no radiation is involved. Berg et al. [40] found that the

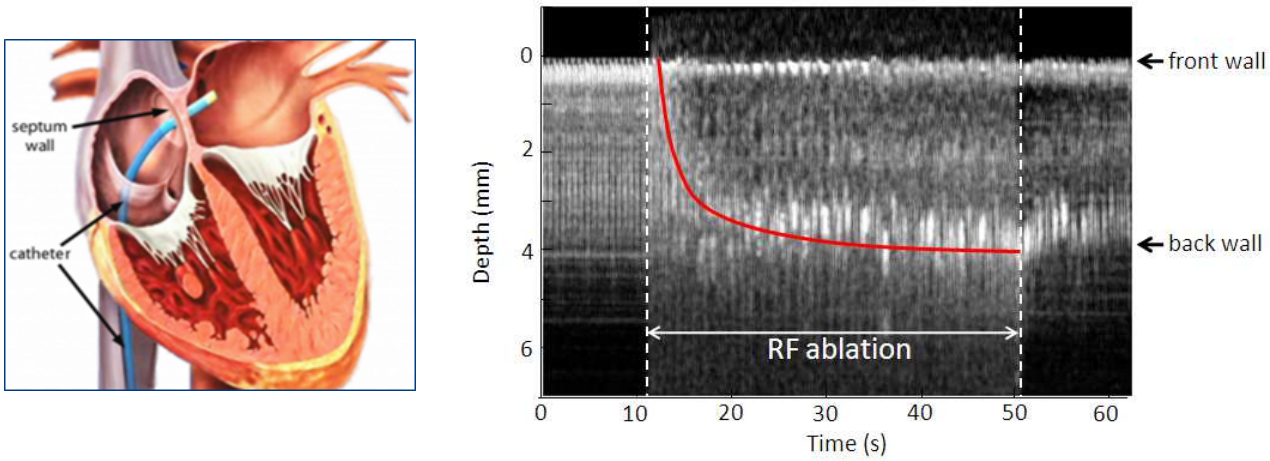

Fig. 1. *(Left)* RF ablation catheter in the heart; *(Right)* An example of lesion created by RF ablation [15], where the red line indicates the change in US image upon energy delivery.

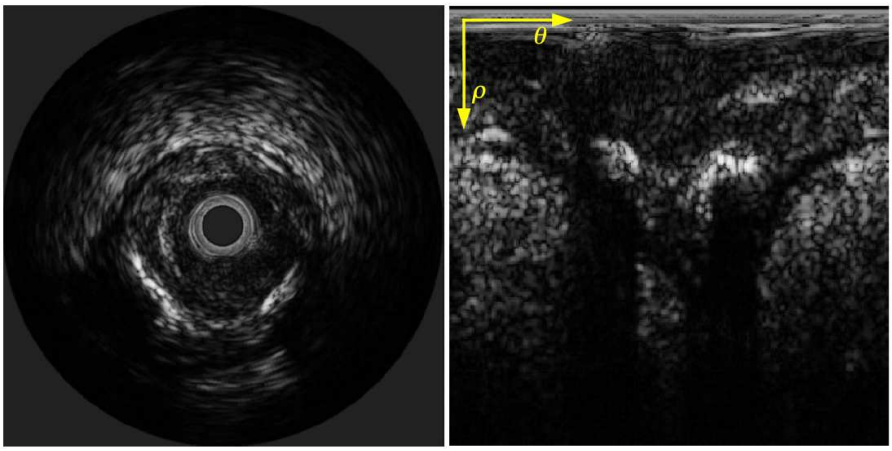

Fig. 2. *(Left)* Standard cross-sectional IVUS image in cartesian coordinates, and *(Right)* its corresponding polar representation: ρ represents the depth in the tissue and θ the position (angle) in the rotation of the probe [35].

supplemental yield of using ultrasound together with mammography was 4.2 cancers per 1000 women screened. Kaplan et al. [41] found 6 (0.36%) extra cancers from 1862 mammgraphic negative patients with dense breasts. However handheld ultrasound breast cancer screening is operator dependent, uneasy to reproduce, time consuming and relatively expensive as a screening procedure when performed by radiologists.

Tissue classification in BUS aims to distinguish benign masses (cysts and fibroadenomas) and malignant cancerous masses. Various approaches have been investigated to detect the suspicious masses in B-mode BUS images [42]–[44], where the challenge is to characterize the textured appearance and geometry of a tumor relative to normal tissue. A survey on cancer detection and classification in BUS images can be found in [39]. Recently, automated 3D breast ultrasound system (ABUS) as a novel modality was proposed to overcome the drawbacks of the traditional 2D ultrasound. Fig. 3 shows one example of an ABUS image. It usually involves a heavy compression from a membrane on the breast. With a swipe of a wide linear or curved transducer, a number of transversal images are generated and reconstructed to become a 3D volume. Different than 2D ultrasound, ABUS provides the possibility of visualizing speculation patterns associated with malignancy on coronal planes. Because of the standard imaging procedure, it is possible to perform temporal analysis on prior and current exams. Since the ABUS images are standardly defined, many researcher paid lots of attention on tumor classification [45]–[49] and cancer detection [50]–[57] using various techniques. Currently GE invenia ABUS system is FDA-cleared for screening purpose [58] while Siemens ABVS system is FDA-cleared for diagnosis purpose [59].

Besides ABUS system which uses reflected echoes, transmission ultrasound is employed for cancer detection and diagnosis as well by FDA-cleared systems such as SoftVue System [60] from Delphinus Medical Technologies and QTscan [61] from QT ultrasound. These systems usually employ rotating ultrasound transducer, to capture details of the tissue of the uncompressed breast for patients positioned in the prone position. Images are generated using both reflection and transmission modalities. The addition of tissue attributes of sound speed and attenuation can enrich diagnostic information for tissue classification.

D. Prostate Cancer

Prostate cancer is the second most common cancer worldwide and the most common malignancy in men [62]. It is due to the abnormal and uncontrolled cell mutation and replication in the prostate gland.

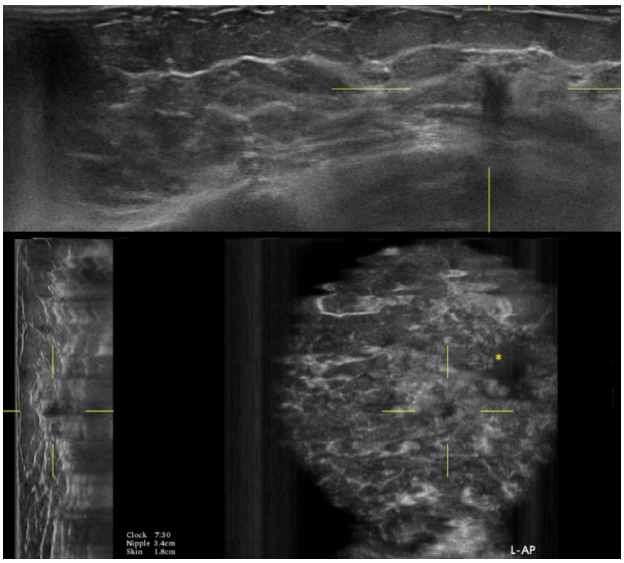

Fig. 3. An example of a lesion in orthogonal planes of an automated 3D breast ultrasound volume [54].

As with any cancer, early detection and treatment is vital for good survival rates of prostate cancer. Although multi-parametric MRI has been increasingly used for prostate cancer diagnosis, transrectal ultrasound (TRUS) is widely used for evaluation of the prostate, because of its advantages of low costs, good availability, and ability to visualize the prostate in real time [63]. TRUS has been used for the early detection and active surveillance of prostatic cancer. Currently, serum prostate-specific antigen (PSA) and Digital Rectal Examination (DRE) are used for screening. If either study is abnormal, TRUS-guided biopsy is performed for diagnostic confirmation [64].

By analyzing the characteristics of the tissue regions, tissue classification in TRUS provides a malignancy map to guide biopsy, which can reduce the number of unnecessary biopsy. However, the prostate regions in TRUS images are characterized by a weak texture, speckle, short gray scale ranges, and shadow regions [8]; detection and delineation of prostate pathology in TRUS is difficult due to the heterogeneous and multi-focal nature of prostatic lesions. Tissue classification has been extensively studied for prostate cancer detection [65]. The earlier work on TRUS tissue classification discriminated the rectangular regions around biopsy needle insertion points with textural features [66]. Later different types of features were considered together with more sophisticated classifiers [67]–[69], for instance, textural features and spectral parameters extracted from RF data were employed in [67]. Morphologic features and multiresolution textural features were also used for malignancy detection [69]. Non-linear Higher Order Spectra (HOS) features and Discrete Wavelet Transform (DWT) coefficients were considered in [70]. It has been shown that combining features extracted from RF analysis of ultrasound signals and texture would result in better classification [65]. HistoScanning [71]–[73] is a commercially-available ultrasound tissue characterisation technique that has shown encouraging results in the detection of prostate cancer.

In addition to gray-scale ultrasound, color Doppler ultrasound (CDUS) has also been used for the evaluation of prostate cancer by detecting the increased perfusion compared with surrounding prostate tissue [63]. It has been shown that the combination of CDUS and gray-scale ultrasound can detect a greater number of prostate cancers than gray-scale ultrasound alone [74]. New ultrasound techniques such as contrast-enhanced ultrasound (CEUS) and ultrasound elastography [74], [75], have been developed to improve the detection of prostate cancer. MRI-ultrasound fusion is another novel imaging technique that is being used to guide prostate biopsy, where the target lesion is marked on the prebiopsy MRI and fused to the real-time TRUS images [76].

The previous two subsections have discussed two main application areas in cancer diagnosis, breast and prostate. Ultrasound tissue classification has also been investigated for diagnosis of other cancer types, for instance, early detection of liver tumour [77]–[80]. Focal liver lesions such as cysts and tumours are concentrated over a quite small area of the tissue and are difficult to identify. The classification of lesions in ultrasound liver image usually depends heavily on the characteristics of the lesions including internal echo, morphology, edge, echogenicity, and posterior echo enhancement. In [77], texture features are used to distinguish malignant and benign liver tumours. Automatic classification of thyroid tissue into benign and malignant types using US are investigated in [81]–[83]; a review on thyroid cancer tissue characterization can be seen in [84].

III. Feature Extraction

The traditional approaches to ultrasound tissue classification start with extracting discriminative features from the ultrasound signal or image. In the US image formation process [1], the radio-frequency (RF) signal acquired by the US transducer undergoes filtering, envelop detection, log compression, and post-processing to finally give a grayscale representation (which is often called A-line). The grayscale signal is then interpolated and rasterized to give a B-mode or M-model image for display.

A large amount of features of different nature have been investigated in the literature for tissue characterization and classification (as summarized in Table I). Here we group them into three categories. The first category relies on tissue appearance in US images, where texture and morphology are usually analyzed. In the second category, the RF signal or envelope-detected data is analyzed. Spectral analysis is often performed to extract characteristics about the behavior (property) of different tissue types in the frequency domain. The last category is to fuse and combine different types of features.

A. Image-based approaches

Before extracting features from US images, image pre-processing and image segmentation are usually performed. Pre-processing consists of speckle reduction and image enhancement (see [39] for some details), and image segmentation is to segment the image into Regions of Interest (ROI) for further analysis [8].

Texture features — Feature extraction from US images aims at describing the appearance of tissue. Most studies have focused on textural properties of speckle which represent the macroscopic appearance of scattering generated by tissue micro-structures [121]. By identifying spatial variations in pixel intensities and quantifying them into numerical features, texture analysis has been widely adopted and different kinds of texture features are available in the literature: Gabor filter responses, derivatives of Gaussian filters, wavelet transform, co-occurrence matrices, Local Binary Patterns, fractal spaces, Markov random fields, and so on. Here we list the texture features that have been widely used for US tissue classification

- Grey Level Co-occurrence Matrix (GLCM) [122]: GLCM is a well-known statistical tool for extracting texture information from images. It measures how often different combinations of pixel intensities occur in an image. GLCM can also be defined as an estimation of the joint probability density function of gray

Feature Type	Feature description	References
Image-based features	GLCM	[67], [85], [86], [87], [32], [88], [89], [81], [90], [77], [91], [92], [42], [93], [43], [94], [83], [95], [47]
	Gabor	[87], [32], [96], [33], [34], [79], [35], [47]
	LBP	[87], [32], [96], [33], [34], [35], [95], [47], [26]
	Wavelet transform	[97], [86], [98], [78], [99], [79], [94], [83], [95], [70]
	Morphological features	[69], [100], [101], [93], [80], [45], [46], [48], [50], [102], [51], [52]
RF-signal-based features	Spectrum-based features	[103], [104], [105], [67], [21], [106], [107], [31], [32], [108], [19], [88], [109], [96], [33], [90], [92], [34], [35], [110], [111]
	RF time series features	[112], [113], [88], [114], [22], [115], [20], [116], [117], [118]
	Statistical distribution modeling	[90], [100], [101], [34], [62], [42], [119]
	Wavelet analysis	[120], [90]

TABLE I
FEATURES FOR TISSUE CLASSIFICATION.

level pairs in an image. Given the co-occurrence matrix, a set of second-order statistic measures can be computed, such as Energy, Entropy, Shade, Promenance and Inertia. The features are also called Haralick features.

- Gabor filters [123]: Gabor filters are obtained by modulating a 2D sine wave with a Gaussian envelope. The characteristics of Gabor filters (wavelets) are similar to those of the human visual system. Representations based on the outputs of Gabor filters at multiple spatial scales and orientations have proven to be successful for texture analysis.
- Local Binary Patterns (LBP) [124]: LBP is an efficient non-parametric method summarizing the local structure of an image. It labels the pixels of an image by thresholding a neighborhood of each pixel with the center value and considering the results as a binary number. The neighborhood of different sizes can be considered to capture dominant features at different scales.

Pujol *et al.* [85] used the GLCM and the cumulative moments [125] to describe texture for tissue and blood classification in IVUS. They have a 96-dimension space for co-occurrence matrices and a 81-dimension space for cumulative moments. After feature selection of Adaboost, 85% feature selected are from the co-occurrence space. In [87], four types of texture features, GLCM, LBP, Gabor filters and the shading of the polar image, are extracted to form a feature vector of 68 dimensions for IVUS tissue classification. In [126] texture analysis and RF signal analysis are compared for IUVS tissue classification. The comparison experiments show that the texture-based approach performs slightly better than the RF signal based approach. Similarly, Escalera *et al.* [32] show that texture features (GLCM, LBP, Gabor, and shadow) outperform the RF features (full spectrum, two global spectral features) and the slope-based features [104]. In [26], different multiscale descriptors were extracted for pixel-level tissue classification on the DU images. Acharya *et al.* [27] extracted 36 types of features using LBP, Fuzzy GLCM, Higher Order Spectra (HOS) features, and others for plaque classification. Similarly, various texture features were considered in [28] for carotid plaque classification.

The second-order co-occurrence features are often supplemented by first order intensity distribution statistics, such as mean, variance, skew and kurtosis. In [91], 23 features from B-mode images are used with a multi-classifier approach for TRUS tissue classification. In addition to GLCM, Maggio *et al.* [90] also extract Unser features and Fractal features to describe image texture. Unser features [127] are statistical attributes generated from the histogram of sum and difference of gray level in US images; both Unser features and GLCM are based on the gray levels distribution statistics. Fractal features [97] is based on the computation of progressive binaried versions of US images obtained through different binary thresholding operations. Spectral features extracted from the RF signals have been used widely for tissue classification. Considering the RF signals may not be available for spectral analysis, the work [68] proposes to extract spectral features from TRUS images, where each ROI is first scanned to form 1-D signals and then spectral features are extracted.

In [86], GLCM and non-separable wavelet transform based features were extracted from US images. In [98] two images are computed from RF signals: (1) a despeckled image containing the anatomic and echogenic information of the liver, and (2) a speckle only image. Intensity features estimated from the despeckled image and texture features (Haar wavelet decomposition) extracted from the speckle only image are used for liver tissue classification. Wan and Zhou [99] extracted features using wavelet package transform from B-mode US liver images. Lee [79] performed multi-resolution analysis by applying m-band wavelet transform and Gabor filters, which decomposes the input US image into sub-images at various resolutions. Then the first and second moments of energy & standard deviation and the fractal dimension are extracted from the sub-images to form the feature vector. Considering pixels in US images are very randomly distributed, which cannot be fully described by second-order measures, Acharya *et al.* [94] utilized the combination of HOS and DWT-based texture features. A range of image texture based features like entropy, LBP, GLCM, and run length matrix were reviewed in [128] for detecting Fatty Liver Disease. Various texture features have been extracted from the thyroid US images for thyroid cancer detection [81], [83].

The image texture in US imaging is intrinsically a function of the micro-structure of tissue and the imaging system [1], as both system effects and tissue micro-structure affect the signal and the speckle

noise [129]. Thus, for the same type of tissue, different system parameters might lead to different texture patterns. This makes the texture-based tissue classification difficult. In clinical practice, to improve the visualization of certain tissue, the physicians often change the US imaging parameters such as contrast, depth and gain. Therefore, in order to extract comparable features belonging to different tissue types, the US images should be normalized. For this purpose, in [87], the raw RF signals were exploited to reproduce ultrasound images with a unique and well controlled set of imaging parameters. Other algorithms could also be designed to make the signal less dependent on acquisition system settings. Texture-based tissue characterization is also strongly dependent on the chosen spatial scale of analysis, so the multi-resolution approaches should be considered [1].

Morphological features — In addition to the above texture features, the morphological features are also often considered for tissue classification in ultrasound. As said above, the texture in US images depends on the imaging system and the acquisition parameters. In contrast, the morphological parameters are less dependent on system parameters and acquisition characteristics, thus more consistent compared to texture features.

The morphological features focus on local characteristics of the tissue region, such as the shape and margin. Compared to texture features, which are calculated from the entire US image or rough ROIs, the morphological features are derived from the segmented ROIs; therefore, the tissue region (such as a tumour) first needs to be segmented. Different morphological features have been considered for tissue classification, e.g., in breast cancer diagnosis [39].

One of the most often used morphological parameters is the depth-to-width ratio (or width-to-depth ratio). Malignant lesions tend to have the ratio bigger than 1 while benign lesions usually have the ratio smaller than 1. This ratio is related to the compressibility of tumour [45]. Due to aggressiveness of the growth, malignant tumours tend to have an irregular shape while benign tumours tend to have a spherical or oval shape. Therefore both sphericity and compactness features [45] are proposed to characterize the irregularity of lesion shapes. Another often used measure is the average orientation of the gray-level gradients along the margin [39].

B. RF-signal-based approaches

The US image formation process, i.e. from raw RF signals to US images, introduces a certain number of approximations (such as envelope detection and log compression), thus a certain amount of information is lost. It is believed that the information lost could be essential in tissue characterization. The features extracted from RF signals are not subject to machine dependent processing, sub-sampling, interpolation, quantization and even operator-dependent settings [35].

Many approaches have been proposed for feature extraction from RF signals [35]. Noble listed in [1] a number of established acoustic and tissue parameters, such as integrated backscatter (IB) coefficient and attenuation coefficient. Below we describe some commonly used features. The physical principles that underpin these features are not our focus, which can be found in the literature.

Spectral features — Following the seminal work of Lizzi *et al.* [103], [130], spectral parameters of local RF signals are the most often used features, based on the hypothesis that different tissue types behave differently in the frequency domain. Lizzi *et al.* studied the relationship of spectral parameters of RF data to tissue microstructure, and proposed to use a few features extracted from the local power spectra for tissue characterization, such as the slope of the linear regression line fitted to the mid-band portion of the spectrum and the intercept of that line at zero frequency. They identified tumours in the eye and liver by using the slope and intercept features [103]. Nair *et al.* [104] extended this approach for coronary atherosclerotic plaque characterization with five additional features: mid-band-fit (MBF, the value of the regression line at the center frequency), maximum and minimum powers, and the corresponding frequencies. Later the integrated backscatter (IBS) coefficient was added [105], which is estimated as the sum of power spectral density over the bandwidth. These methods are known as seven-feature or eight-feature approach in the literature. It should be mentioned that there is a linear dependence among the first three spectral features: slope, intercept, and MBF, since one can be derived from the other two. The same dependence can be derived for IBS and MBF, since MBF is the first-order approximation of IBS [107]. Mean central frequency has also been considered for tissue classification, which is the first moment of the bandwidth of the power spectrum. It captures the shifting of RF signal central frequency due to attenuation. Spectral features are calculated based on the estimated local power spectrum of RF signals, which can be computed by using the Fourier transform or by the AutoRegressive (AR) model. It is shown that the AR method can provide a more stable spectral approximation for small signal window [87]; however, the accuracy of AR method is influenced by the sampling frequency, order and window size [107]. Feleppa *et al.* [106] pioneered the usage of RF spectrum analysis for prostate cancer detection. Liu *et al.* [131] extended the 1D spectrum analysis to 2D power spectra analysis [109], where the approach was shown to outperform 1D spectrum analysis. In [19], spectral features including intercept, slope, and MBF were considered for the HIFU lesion characterization. To differentiate different cardiac tissue types, thirteen spectral parameters were computed from the power spectrum of the RF data in three different bandwidth ranges [11]. Autoregressive models of order 4 were used as they provide effective estimates of the power spectrum for short-time data.

Katouzian *et al.* [107] investigated the consistency and reliability of the eight-feature approach for plaque tissue characterization. Their study demonstrated that the spectral features are sensitive to variations in the transducer parameters and other factors (such as window size and the order of the AR model). They presented a full-spectrum analysis to extract the spectral magnitudes at every frequency bin within the functional range of bandwidth. In addition, the energy norm of spectral signals and the radial position of the tissue sample from the center of the transducer (in the IVUS image) were considered as features. Their experiments show that the full-spectrum analysis delivers superior performance for plaque classification. Similarly, in [31], the plaque tissues are classified by comparing the full spectrum of a tissue sample to the ones in the training database. As illustrated in Figure 4, the local spectrum was computed by averaging the magnitude of the windowed spectrum, where the Enclidean distance is calculated as the measure of similarity. In [110], the full spectrum of RF signals (averaged over the ROI) were considered for prostate tissue classification. Instead of using the entire length of the spectrum, Laplacian eigenmaps was employed for reducing the dimensionality of the spectral feature space.

RF time series — RF time series analysis has been proposed for tissue typing [20], [88], [112], [113], [118], based on the assumption that the time series of echo signals carry tissue type information. "Time series" refers to RF signals collected over a certain time interval at a fixed spot (pixel/voxel) of tissue [88], as shown in Figure 5. The signals are recorded while the imaging probe and tissue are fixed. For a given ROI, to extract features from RF time series, the

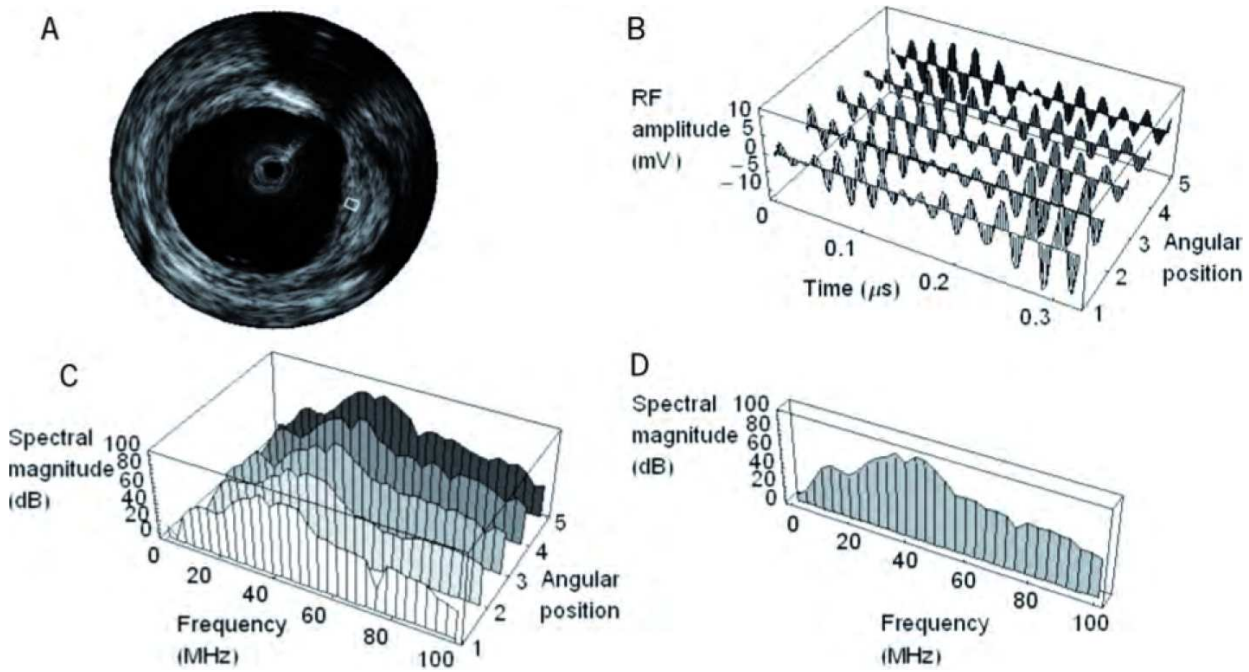

Fig. 4. Computing the local spectrum [31]. A specific ROI on an IVUS image is shown in (a). The raw RF signals along 5 adjacent A-lines comprising this ROI are graphically represented in (b). The individual spectrum corresponding to these RF signals are shown in (c). The average of these 5 spectra yields the spectrum shown in (d). This local spectrum encodes information about the tissue within the ROI.

mean of the time series from all spatial samples in the ROI is first deducted to obtain the zero-mean time series, where the length of time series is zero-padded to the closest power of 2. After calculating the power spectrum of RF time series for each spatial sample in the ROI, the spectrum is averaged over the ROI, so the ROI is represented by a single "averaged" power spectrum, which is further normalized by dividing by its maximum. Then various features can be extracted, for instance, the sums of the power spectrum at four frequency bands, the slope and intercept of the best-fit line to the entire power spectrum, the fractal dimension, and so on (see [20] for details). Although these features are also computed based on spectral analysis of RF signals, they are fundamentally different from the spectral features discussed above. The spectral features described earlier are computed using power spectrums of segmented RF scan lines in one frame. In contrast, the RF time series approach analyzes the local variability of RF signals in time, and the features are computed based on spectral analysis of temporal samples of RF signals originating from the same spatial location.

Moradi *et al.* [88] presented quantitative comparisons on the RF time series features, spectral features (intercept, slope, and mid-band-fit), and texture features (GLCM and statistical moments of pixel intensities) for ex-vivo prostate cancer detection. Their experiments show that RF time series features outperform the spectral features and texture features. In the absence of physiologic motion in ex-vivo experiments, the tissue typing characteristics of RF time series were potentially due to the minute temperature changes caused by continuous sonification. The hypothesis was investigated in [132], [133]. In [20], the RF time series signals prior to, and at the end of the ablation process are analyzed for lesion detection. RF time series features are exploited in [116] for in-vivo prostate cancer detection. In [117], two features out of nine (seven spectral features described above, one wavelet-based feature and mean central frequency) were selected by a recursive feature elimination process for prostate cancer detection.

Statistical distribution modeling — The backscattered signals can be treated as random samples. Modeling their probability density function with appropriate statistical distributions [134] can reflect the backscattering properties, which are dependent on the scatterers in tissue. The parameters of such a distribution can be used as features for tissue classification. Different models have been developed to simulate the backscattered echo. The Nakagami distribution has been widely used as a general model for envelope backscattered data under different scattering conditions and scatterer densities [1]. The Nakagami parametric image [42], [100], [101] based on the Nakagami model has been shown to be useful for discriminating between benign and malignant breast tumours. In [119], the echo signal is represented as a mixture of Nakagami distribution, where the mixture model is learned using the random forest algorithm. Maggio [62] proposed a sampled continuous-time autoregressive moving average (CARMA), and utilized CARMA parameter for tissue characterization. The Rayleigh distribution is also widely used to describe homogeneous areas in US images. For tissue with heterogeneous regions (e.g. plaque), more complex distributions are needed. In [34], [135], Seabra *et al.* proposed to use the Rayleigh mixture model (RMM) to model the plaques in IVUS. Their experiments show that the mixture coefficients and Rayleigh parameters can describe different plaque types.

Wavelet analysis — Multi-resolution analysis of RF signals by wavelets has been studied, and the wavelet coefficients can be used for tissue classification. This approach has been proved to be appropriate for plaque characterization in IVUS [35]. The authors in [120] utilized multi-scale products of wavelet transform sequences of RF signals to estimate the scatter distribution in the tissue, which is used for prostate cancer detection. In [90], the wavelet coefficients of RF signal, their polynomial fitting and the coherent and diffuse components obtained by signal decomposition were exploited for TRUS tissue classification.

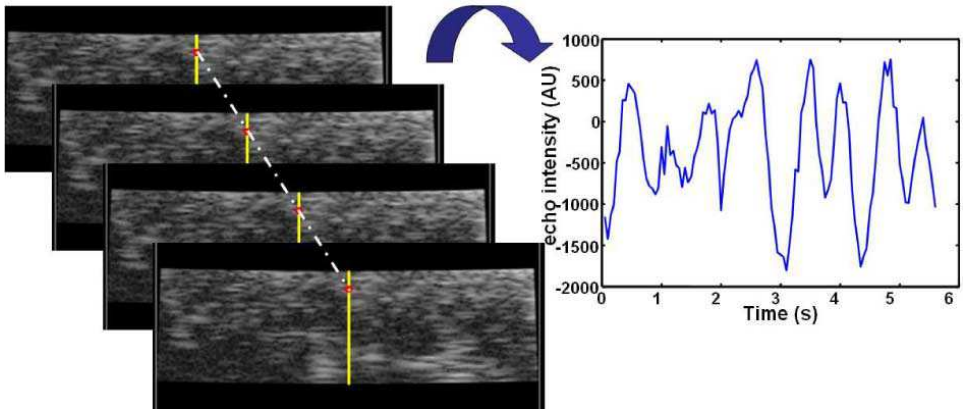

Fig. 5. Samples of RF signals collected over time from a fixed spot of tissue under emission of sequential ultrasound form one RF time series [88].

Beyond the feature categories discussed above, other features such as scatterer size and the speed of sound can also be considered. Although the mean speed of sound in biological tissue is normally assumed to be 1540m/s, it is known that the ultrasound wave propagates with different speed in tissue with different density. The estimation of speed of sound has been proposed as an indicator of tissue abnormality [1]. Another related parameter is acoustic impedance. Given the relationship between the acoustic impedance and the tissue density, the relative acoustic impedance can be used as a parameter for tissue characterization [35].

C. Feature Combination and Selection

Individual features usually have limited discriminative power. Combining different features can potentially provide better tissue discrimination, as the features of different nature might provide complementary information. Therefore, feature combination has been exploited in many studies [1]. Escalera *et al.* [32] considered texture features (GLCM, LBP, Gabor, and shadow), RF-based features (full spectrum, two global spectral features), and slope-based features [104] for tissue classification in IVUS. In [33], [96], both texture features (Gabor, LBP, and shadow) and spectral features from RF signals are extracted for plaque characterization in IVUS. In another study [34], the combination of texture and spectral features with the RMM features achieves the superior performance in IVUS tissue classification. Multiple features including statistical parameters, spectral features from RF signals, and texture features from B-mode images are considered in [90] for TRUS. In [88], the texture and spectral features in combination with the RF time series features result in the best performance. It is concluded in [65] that combining features extracted from RF signals and image textures provide better prostate tissue classification. In [100], [101], the morphological features (e.g. contour) are combined with the Nakagami parametric image to characterize benign and malignant breast tumours. In another study [42], the GLCM features are combined with the Nakagami parametric image for breast tumour detection. Acharya *et al.* [83] extracted GLCM texture features and discrete wavelet transformation (DWT) features from the thyroid US images for thyroid cancer detection.

Feature combination inevitably increases the dimension of the feature vector. In practice, the combined features could be redundant for tissue characterization. Furthermore, high dimensionality requires more complex classification models which tend to overfit the training data. So it is essential to select an optimal feature set with low dimensionality containing only significant and non-redundant features. Feature selection approaches can be categorized into two classes: filter and wrapper. Filter methods select features according to a score that measures the importance of a feature with respect to the tissue type, and does not take into account the classification algorithms. Typically the ranking criterion can measure distance, information, dependency, or consistency between features and tissue type. For example, mutual information was exploited in [90] for feature selection. Unsupervised learning methods such as principal component analysis (PCA) can also be used to reduce redundancy in features [88]. In contrast to filter methods, wrapper methods select features based on the performance of a classifier on the feature set, thus they are classifier-dependent. Pujol *et al.* [85] adopted Adaboost to select the most discriminative texture features for IVUS tissue-blood classification. In [68], feature selection using particle swarm optimization is adopted to select the optimal spectral feature subset. In [117], two features were selected from nine RF time series features by a recursive feature elimination process, based on their weight in a linear SVM classifier. It is also possible to select features using a hybrid method, to take advantages of both filter and wrapper methods. For instance, a mutual information hybrid feature selection algorithm is presented in [90] for TRUS tissue classification.

IV. Classifier Design

After feature extraction, the next step is to design a classifier to automatically label tissue types based on the features. Due to the large variations in US images (signals), most features have low discriminative power and it is often difficult to find a boundary separating different tissue types in the feature space. Machine learning approaches could be powerful for tissue classification, which can handle variations in the US data by training a classifier from a large database of examples. A new tissue sample is then be classified using the learned classifier.

As summarized in Table II, different classifiers have been exploited for tissue classification, for instance, various classification approaches for liver tissue classification are reviewed in [128]. In earlier studies [104], decision trees, neural networks, and fuzzy systems were utilized. Later Support Vector Machines (SVM) have become a popular classifier. In this section, we discuss a few widely-used classifiers. It is worth mentioning that classification performance should be compared with caution, because there is significant variability in the training and evaluation data sets, as well as evaluation settings and ground truth used, among these studies.

Discriminant Analysis — Linear discriminant analysis (LDA) and logistic regression are frequently-used linear classifiers. Logistic regression is a model for predicting the probability of an event occurring as a function of other factors. LDA [140], also called Fisher

Classifier	References
Linear classifier	[107], [42], [136], [93]
Neural Network	[106], [112], [108], [78], [91], [114], [79]
k-NN	[107], [137], [78], [79]
Decision Trees	[66], [104], [105], [94]
Bayes classifier	[97], [113], [98], [78], [91]
SVM	[86], [68], [69], [88], [120], [89], [77], [99], [91], [62], [79], [82], [22], [115], [20], [133], [80], [116], [117], [111], [70], [26]
Adaboost	[85], [87], [96], [33], [34], [35], [83]
Random Forest	[31], [138], [119], [117], [139]

TABLE II
CLASSIFIERS FOR TISSUE CLASSIFICATION.

discriminant analysis, searches for the projection axes on which the data points of different classes are far from each other while requiring data points of the same class to be close to each other.

The linear classifiers are fast and easy to implement but cannot capture the nonlinear separation of different classes. Especially when features of different nature are used, a nonlinear classifier can achieve better accuracy [65]. Katouzian *et al.* [107] exploited linear Fisher classifier for IVUS plaque characterization, and showed that the linear classifier cannot discriminate different tissue types because of the overlap among different classes. Maggio *et al.* [90] exploit a multi-feature nonlinear classifier based on generalized discriminant analysis (GDA) with Gaussian kernels for prostate cancer detection, which delivers superior classification performance.

Support Vector Machine — SVM [141] is a discriminant method based on the Bayesian learning theory. SVM performs an implicit mapping of data into a higher dimensional feature space, and then finds a linear separating hyperplane with the maximal margin to separate data. SVM has been widely used for tissue classification [82], [86], [89], [99], [110], for example, SVM was used to differentiate steatosis and non-steatosis liver specimens [86]. Horng [89] adopted multi-class SVM to classify US images of supraspinatus. Wan and Zhou [99] used a SVM classifier with texture features extracted from B-mode US images for live tissue classification, and their approach results in an accuracy of 85.79% on classifying 702 normal and 200 cirrhosis liver images. Similarly, SVM was used with the statistical and textural features extracted from thyroid elastograms for thyroid cancer characterization [82]. In [110], after dimensionality reduction of full spectrum, SVM classification was performed for separating cancer from normal prostate tissue. SVM has also been used with RF time series features for prostate cancer detection [88], [116], [117]. Also using RF time series features, SVM is used to classify ablated and non-ablated tissue [20], achieving the accuracy of 84.4% for the leave-one-out cross-validation on the 12 *ex vivo* tissue samples.

Adaboost — Adaptive Boosting (Adaboost) [142] provides a simple yet effective approach for stagewise learning of a nonlinear classification function. It combines the feature selection and classifier training steps in one process. Adaboost learns a small number of weak classifiers whose performance is just better than random guessing, and boosts them iteratively into a strong classifier of higher accuracy. In [85], Adaboost with decision stumps was possibly for the first time utilized for tissue classification, where texture features were selected to build a strong classifier for IVUS tissue characterization. Later it was used in [33]–[35], [87]. In [83], with perceptron as weak learner, Adaboost was used with texture features to distinguish benign and malignant thyroid nodules.

Random Forest — Random forests [143] are another ensemble learning method, which operate by constructing a multitude of decision trees using the training data and then classifying a testing sample as the majority prediction of the individual trees. Random forests can handle a large amount of training data efficiently. In [138], random forests were adopted to classify tissue in 3D echocardiography. Sheet *et al.* [119] utilized random forest to identify different types of tissue in IVUS using statistics features extracted from US signals. Random forests were also exploited for prostate cancer diagnosis [117]. In a recent work [11], thirteen spectral parameters derived from the power spectrum of the RF data were used in generating random forests for cardiac tissue classification. The random forest classifier with 50 classification trees resulted in an overall accuracy of 92.4%, sensitivity of 91.1%, specificity of 93.9%. The result demonstrates the potential of echocardiography and spectral analysis techniques in differentiating cardiac adipose tissue, myocardium, and blood.

In [31], the tissue classifier contains a bank of tissue detector arrays, e.g., 10 for each tissue type. Each tissue detector array consists of a number of (e.g. 5) basic tissue detectors tuned to a particular tissue type, where the basic tissue detector performs binary classification using a small database of the particular tissue type and other types (e.g. necrotic vs. non-necrotic tissue). The tissue detector in the same array contains similar (but not identical) small database of spectra. Rather than designing a single tissue detector array by utilizing all available training data, the authors design several detector arrays by utilizing randomly selected subsets of the training data. Finally, given an input spectrum, the classifier makes the final decision based on the outputs of the detector arrays using a Bayesian classifier. Having a large and diverse collection of independently designed classifiers is known to produce a more accurate classifier. In this respect their method share similarities with the random forests algorithms. Their approach can classify four types of IVUS tissue, namely necrotic, lipidic, fibrotic and calcified tissues, with an accuracy of 97%, 98%, 95% and 98%, respectively.

Other Classifiers — The *k*-Nearest Neighbors (*k*-NN) classifier is a widely-used non-parametric method for classification. Given a sample, *k*-NN computes its distance with every data sample in the training set, and assign it to the most frequently occurring class

among the top k nearest neighbors. The k-NN classifier can capture complex boundary among different classes but it is computationally expensive. Katouzian *et al.* [107] exploited k-NN for IVUS plaque characterization. In [78], the k-NN, neural network, and Bayes classifier were utilized to classify liver tissues. An adaptive subspace self-organizing map was used in [137] to extract features from IVUS RF signals, and the classification is done by considering similarities among the distributions of feature vectors using the Mahalanobis's generalized distance. In [32], Escalera *et al.* presented a sub-class Error Correction Output Codes (ECOC) method [144] for multi-class tissue classification, which splits the original set of classes into sub-classes. A binary discriminative learning technique based on the approximation of the nonlinear decision boundary by a piecewise linear smooth additive model was proposed in [145] for IVUS tissue classification. In [98], a Bayes classifier was adopted to classify fatty live tissue, using image features extracted from a despeckled image and a speckle only image. This approach achieves an accuracy of 95% on an image set of 20 images (10 normal liver and 10 fatty liver samples). In [108], with spectrum analysis of RF signals, four non-linear classifiers were trained for prostate tissue classification: multi-layer-perceptron neural networks, logitboost algorithms, SVM, and stacked restricted Boltzmann machines. By embedding ECOC in the potential functions for Discriminative Random Fields (DRF), Ciompi presented in [35] a multi-class classification technique called ECOC-DRF for IVUS tissue classification. In [43], the segmented ROI in breast US images is viewed as a bag, and sub-regions of the ROI are considered as the instances of the bag. Multiple-instance learning is then adopted for breast tumour classification. Acharya *et al.* [94] adopted a decision tree classifier and US image features for classifying normal and abnormal liver tissue.

Combination of Classifiers — Each individual classifier has inherent limitations, e.g., uncertainty with respect to a particular class. One classifier may provide a clearer conception of a class than other classifiers do [79]. The samples misclassified by various classifiers do not necessarily overlap. Therefore, different classifiers can potentially offer complementary information, and the combination of various classifiers could improve the performance. These observations have motivated the interest in combined classifiers. In [79], an ensemble of classifiers was adopted by combining the outputs of various classifiers based on fuzzy integral. More specifically, the fuzzy k-nearest neighbor classifier, the probabilistic neural network, the back-propagation neural network, and SVM were combined. The experiment results showed that the proposed ensemble of classifiers achieves performance superior to that obtained with any single classifier. Similarly, a multi-classifier system was adopted in [91] to improve the prostate cancer diagnosis as compared to individual classifiers. In [13], an ensemble machine-learning model with 3 algorithms (support vector machines, random forests, and artificial neural networks) was investigated for tissue classification using STE features in 2D echocardiography.

V. Deep Learning Approaches

Nowadays deep learning has become popular as a self-taught approach in which features are computed in an automatic manner instead of combining manual designed features. These approaches rapidly become state-of-the-arts that outperform other traditional methods in ultrasound. The popular techniques include convolutional neural networks (CNN), recurrent neural networks (RNN), and unsupervised learning approaches. Although comprehensive surveys on deep learning in medical image analysis or ultrasound image analysis already exist [146], [147], in this section, we aim for introducing notable research specifically on deep learning for tissue classification.

Convolutional Neural Networks (CNN) — Convolutional neural network is the most popular and successful deep learning architecture. In 2012, it was re-introduced by Alex Krizhevsky *et al.* [148] and achieved huge success in the ImageNet competition [148]. A typical CNN contains several pairs of a convolution layer and a pooling layer. The intermediate outputs of these layers are fully connected to a multi-layer perception neural network. Later, new tricks were proposed including dropout [4], batch normalization [5] and resnet block [6]. The purpose of dropout is to solve over-fitting caused by co-adaptations during training. Dropout technique improves the performance of neural networks. Batch normalization helps to accelerate the training of deep networks by normalizing activations and achieve the same accuracy with 14 times fewer training steps [5]. It also improved the best published result on ImageNet classification with an ensemble of batch-normalized networks. Resnet block was proposed in [6], where they found out that identity shortcut connections and identity after addition activation are important for smoothing information propagation [149]. Huang et al. [150] proposed DenseNet (Fig. 6) which is a network architecture where each layer is directly connected to every other layer in a feed-forward fashion. For each layer, the feature maps of all preceding layers are treated as separate inputs whereas its own feature maps are passed on as inputs to all subsequent layers. This connectivity pattern yields state-of-the-art accuracies. DenseNet achieves similar accuracy as ResNet, but using less than half the amount of parameters and roughly half the number of FLOPs.

As an extension of CNN, fully connected convolutional networks (FCN), such as U-net architecture [151], have gained propitiatory for the segmentation tasks. The U-net can be recognized as two parts, the descending part and the ascending part, with a number of convolutional layers. It consists of a number of downsampling steps followed by the same number of upsampling steps. Skip-layer connections exist between each downsampled feature map and the commensurate upsampled feature map. The activation function can be rectified linear unit (ReLU). The FCN aims to construct a feature map for each image, from which object-relevant information will be extracted and object-irrelevant information will be discarded.

Both CNN and FCN have been applied extensively in ultrasound. Quite often, the deep learning techniques are combined with post-processing or other traditional techniques to boost the classification performance. In ultrasound images, both patch-based approach [152], [153] [154] [155] [156] [157] [158] [159]–[161] [162] [163] and FCN [164] [165] [166]–[169] [170] [171] [172]–[177] [178], [179] are applied in various applications. In [180] [181], the CNN was used with shape modeling to achieve better performance.

A big advantage of CNN is that when the number of training images increases, the performance of the network improves. On the other hand, the training of a deep learning model would also require a large amount of labeled data. In many medical image classification cases, the number of labeled data are limited for training. Transfer learning has been proposed [182] to effectively tackle the problem of limited availability of the labeled data. Transfer learning literally means that experience gained from one subject can be transferred to other subjects. In neural networks, it means that the parameters trained on one dataset can be reused for a new dataset. Usually, the first n layers of a pre-trained networks are copied to the first n layers of a new network. The remaining layers of the new network are initialized randomly and trained according to the new task [183]. In ultrasound, transfer learning is used in fetal ultrasound [184], [185], pelvic ultrasound [186] including prostate cancer detection [187], breast cancer classification [188], thyroid nodules classification

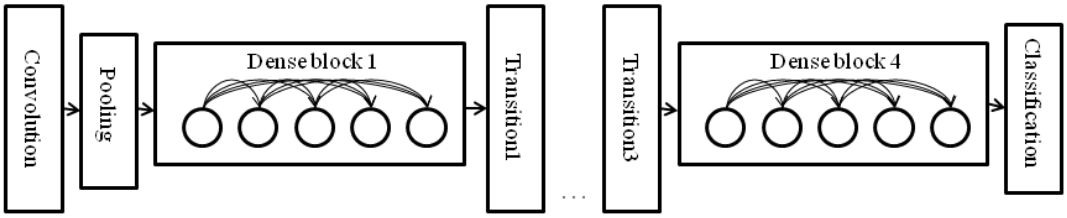

Fig. 6. Demonstration of Densenet 121.

[189], [190], liver fibrosis classification [191], cardiac ultrasound [192], bone detection [193] and abdominal classification [194].

Recurrent Neural Networks (RNN) — Recurrent neural networks [195] are often used to process a sequence of data. It is a class of neural networks where the connecting nodes are one way connected. The node in its sequence receives inputs using the computation of previous nodes. Therefore RNN is capable of having "memory". Long short-term memory (LSTM) is a type of RNN which avoids the vanishing gradient problem [196]. It uses special units in addition to standard units that can maintain information in memory for long periods of time. Therefore it can learn longer-term dependencies. Because of its "memory" and the capabilities of processing data of an arbitrary length. RNN is quite popular for speech recognition and hand-writing recognition.

In ultrasound imaging, the image sequence can be acquired in real time and therefore it is suitable to apply RNN for the learning tasks such as tissue identification of different temperature during HIFU ablation therapies, diseased tissue classification with Doppler ultrasound [197], and cancer tissue detection in temporal enhanced ultrasound [198]. For static ultrasound images, it is also quite often that static images are serialized into dynamic sequences and then processed with RNN and the results are often robust compared to conventional CNN schemes [185], [199].

Unsupervised and Weakly Supervised Learning — In medical imaging, due to scarce of the manual efforts, it is not always applicable to create a large amount of labeled data to directly apply deep learning based classification. Therefore unsupervised schemes have been proposed. Restricted Boltzmann machine [200], [201] and auto-encoders [202]–[206] are invented to learn the feature representation of the data without labeling. Autoencoders learns a representation of the inputs and is deterministic while Restricted Boltzmann machine learn the statistical distribution and is generative and it can also generate new data with given joined distribution. An active area of unsupervised learning is to extract representative features for cancer classification in prostate [207], [208], breast [208], [209] and liver [210]. The unsupervised learning extracts the high-level features representation from cancer regions. These features are the inputs for classifiers such as support vector machine and K-nearest neighbor. Weakly supervised method is a learning method which makes the use of image-level labels in the situation where pixel-level annotations are not available. van Sloun and Demi [211] applied a weakly supervised method based on a fully convolutional neural network for automatically detecting and localizing B-lines artefacts in lung ultrasound.

Table III summarizes the latest deep learning techniques applied in ultrasound.

VI. FDA-cleared machine learning algorithms

Outside the research regime, there are FDA cleared tissue classification algorithms or products are being accepted in the clinic to benefit patients in real practice.

In breast imaging, lesion classification products by Koios Medical [212] for AI-based clinical decision support in 2D ultrasound have received clearance. This will aid radiologists to be more selective on biopsies. The breast cancer detection product in automated 3D breast ultrasound by Qview Medical [213] has been proven to be effective in terms of diagnosis and efficient in terms of reading time.

In cardiac imaging, FDA recently approved the first AI-guided medical imaging tool by Caption Health [214] for the use in cardiac ultrasounds in which tissue-classification algorithms are behind. The tool can automatically capture video clips, and saves the best video clip acquired from a particular view for reviewing.

In spine imaging, Tissue Differentiation Intelligence [215] received clearance for the company's SonoVision ultrasound platform which visually differentiates nerve, muscle, bone, and vessels in real-time and facilitate the surgical operations.

In prostate imaging, Focal Healthcare provides a FDA-cleared solution [216] for MR guided ultrasound biopsy for identifying cancer tissues which help urologists perform fusion biopsy procedures more efficiently and accurately.

VII. Discussions

Compared to techniques in computed tomography (CT), magnetic resonance (MR) and X-rays, the techniques of tissue classification in ultrasound are less applied. The main reason might be the lack of consistency across acquired ultrasound images which boils down to the problem of user-dependency of applying ultrasound imaging. Ultrasound quality is operator dependent and subjective to imaging parameters, positioning of probes, compression of the probes on tissues. These factors lead to different looks of ultrasound images while the robustness of the tissue classification will depend on the similarity of training data for developing the techniques and the testing data in clinical practice. To alleviate this problem, the best approach is to improve the standardization of the imaging via technology or guideline to make the procedure less-user dependent and image-looks consistent.

Combining different imaging modalities is a promising direction for better tissue classification, for example, combining elastography with contrast-enhanced ultrasound is studied in [217]. Compared to using elastography alone, in an 86-patient study, this approach decreases the false-positive rate from 35% to 10%, and improves the positive predictive value from 65% to 90%. For prostate cancer, the fusion of TRUS and MRI for biopsy guidance may offer improved results by combining the strengths of the two imaging modalities [218]. In [111], ovarian tissue features extracted from photoacoustic spectra data, beam envelopes and co-registered ultrasound and photoacoustic

Deep learning techniques	Organ	Ultrasound imaging	References
CNN	Fetal	B-mode	[184], [185] [157], [160] [170] [158]
CNN	Pelvic	B-mode	[186]
CNN	Carotid	B-mode	[155]
CNN	Breast	B-mode including ABUS	[165] [172], [173], [175]–[177] [178]
CNN	Musculoskeletal	B-mode	[162]
CNN	Liver	B-mode	[163]
CNN	Liver	Contrast enhanced ultrasound	[152]
CNN	Prostate	Contrast enhanced ultrasound	[156]
CNN	Heart	B-mode	[153], [168] [154], [161] [174], [179], [192]
CNN	Prenatal	B-mode	[167]
CNN	Lymph node	B-mode	[164]
CNN	Breast	B-mode	[165]
CNN	Brain	B-mode	[169]
CNN	Thyroid	B-mode	[159] [181], [189], [190]
CNN	Bone	B-mode	[193]
RNN	Ophthalmic artery	Doppler ultrasound	[197]
RNN	Prostate	Contrast-enhanced ultrasound	[198]
Unsupervised learning	Prostate	B-mode	[207], [208]
Unsupervised learning	Breast	B-mode	[208]
Unsupervised learning	Breast	Shear-wave elastography	[209]
Weakly supervised learning	Lung	B-mode	[211]

TABLE III
DEEP LEARNING TECHNIQUES FOR DIFFERENT ULTRASOUND APPLICATIONS.

images are used to characterize cancerous vs. normal tissue using a SVM classifier.

One of the critical issues in tissue classification research is the creation of a reliable data set with ground truth. Large databases are necessary for training powerful classifiers and validating the trained classifiers. To fairly evaluate different tissue classification approaches, large benchmark databases should be used. However, currently, large standard databases for public use are absent, also for the very common and highly diagnosed diseases such as prostate cancer or breast tumour. Most existing studies were performed by using their own data sets, which usually have different sizes and different tissue types, acquired using different sources and settings. Therefore, more efforts should be put on collecting large databases with ground truth and making them publicly available for research. In [62] a database with ground truth for prostate cancer was collected.

Another challenge for some clinical applications (e.g. IVUS and cardiac ablation) is how to obtain ground truth for the acquired data. Currently, the ground truth is mainly obtained by expert annotations or the histopathological analysis, which is a slow and complex process, leading to limited data with annotation. For machine learning, a semi-supervised learning scheme can be considered, to use both labelled and unlabelled tissue samples for training. In [33], [96], an approach was presented to enhance the *in vitro* training data set by selectively including examples from *in vivo* data for plaque characterization. The enhanced classifier performs well on both *in vitro* and *in vivo* data.

In future work, a better understanding and modeling of tissue characteristics in the presence of artefacts, and the design of more powerful classification approaches that can handle uncertainty and variations in the US data will be research focus. Deep learning [219] applied to the huge amount of US data acquired in clinical practice remains a topic to explore.

VIII. CONCLUSIONS

This paper has presented a survey on ultrasound tissue classification, particularly focusing on recent development in this area. After introducing the main clinical applications, both the traditional approaches, which consists of feature extraction and classifier design, and the recent deep learning approaches are reviewed. Though much progress has been made in the last years, there are remaining challenges for automatic tissue classification in ultrasound.

REFERENCES

[1] J. Alison Noble. Ultrasound image segmentation and tissue characterization. *Proc. of the Institution of Mechanical Engineers, Part H: Journal of Engineering in Medicine*, 224(2):307–316, 2010.

[2] Johan M. Thijssen. Ultrasonic speckle formation, analysis and processing applied to tissue characterization. *Pattern Recognition Letters*, 24(4-5):659–675, 2003.

[3] Alex Krizhevsky, Ilya Sutskever, and Geoffrey E Hinton. Imagenet classification with deep convolutional neural networks. In *Advances in neural information processing systems*, pages 1097–1105, 2012.

[4] Nitish Srivastava, Geoffrey E Hinton, Alex Krizhevsky, Ilya Sutskever, and Ruslan Salakhutdinov. Dropout: a simple way to prevent neural networks from overfitting. *Journal of machine learning research*, 15(1):1929–1958, 2014.

[5] Sergey Ioffe and Christian Szegedy. Batch normalization: Accelerating deep network training by reducing internal covariate shift. In *International Conference on Machine Learning*, pages 448–456, 2015.

[6] Kaiming He, Xiangyu Zhang, Shaoqing Ren, and Jian Sun. Identity mappings in deep residual networks. In *European Conference on Computer Vision*, pages 630–645, 2016.

[7] Mohammed A. Moharram, Regis R. Lamberts, Gillian Whalley, Michael J. A. Williams, and Sean Coffey. Myocardial tissue characterisation using echocardiographic deformation imaging. *Cardiovascular Ultrasound*, 17(27), 2019.

[8] J. Alison Noble and Djamal Boukerroui. Ultrasound image segmentation: a survey. *IEEE Transactions on Medical Imaging*, 25(8):987–1010, 2006.

[9] M R Milunski, G A Mohr, J E Prez, Z Vered, K A Wear, C J Gessler, B E Sobel, J G Miller, and S A Wickline. Ultrasonic tissue characterization with integrated backscatter. acute myocardial ischemia, reperfusion, and stunned myocardium in patients. *Circulation*, 80(3):491–503, 1989.

[10] David L Prior, Jithendra B Somaratne, Alicia J Jenkins, Michael Yii, Andrew E Newcomb, Casper G Schalkwijk, Mary J Black, Darren J Kelly, and Duncan J Campbell. Calibrated integrated backscatter and myocardial fibrosis in patients undergoing cardiac surgery. *Open Heart*, 2(1), 2015.

[11] Akhila Karlapalem, Amy H. Givan, Maria Fernandez del Valle, Miranda R. Fulton, and Jon D. Klingensmith. Classification of cardiac adipose tissue using spectral analysis of ultrasound radiofrequency backscatter. In Brett C. Byram and Nicole V. Ruiter, editors, *Medical Imaging 2019: Ultrasonic Imaging and Tomography*, volume 10955, pages 101 – 108. International Society for Optics and Photonics, SPIE, 2019.

[12] Nobuyuki Kagiyama, Sirish Shrestha, Jung Sun Cho, Muhammad Khalil, Yashbir Singh, Abhiram Challa, Grace Casaclang-Verzosa, and Partho P. Sengupta. A low-cost texture-based pipeline for predicting myocardial tissue remodeling and fibrosis using cardiac ultrasound. *EBioMedicine*, 54, 2020.

[13] Sukrit Narula, Khader Shameer, Alaa Mabrouk [Salem Omar], Joel T. Dudley, and Partho P. Sengupta. Machine-learning algorithms to automate morphological and functional assessments in 2d echocardiography. *Journal of the American College of Cardiology*, 68(21):2287 – 2295, 2016.

[14] Chayakrit Krittanawong, Anusith Tunhasiriwet, HongJu Zhang, Zhen Wang, Mehmet Aydar, and Takeshi Kitai. Deep learning with unsupervised feature in echocardiographic imaging. *Journal of the American College of Cardiology*, 69(16):2100 – 2101, 2017.

[15] Matthew Wright, Erik Harks, Szabolcs Deladi, Freek Suijver, Maya Barley, Anneke van Dusschoten, Steven Fokkenrood, Fei Zuo, Frédéric Sacher, Méléze Hocini, Michel Haïssaguerre, and Pierre Jaïs. Real-time lesion assessment using a novel combined ultrasound and radiofrequency ablation catheter. *Heart Rhythm*, 8(2):304–312, 2011.

[16] Hongxu Yang, Caifeng Shan, Arash Pourtaherian, Alexander F. Kolen, and Peter H.N. de With. Catheter segmentation in three-dimensional ultrasound images by feature fusion and model fitting. *Journal of Medical Imaging*, 6(1):015001, 2019.

[17] Hongxu Yang, Caifeng Shan, Alexander F. Kolen, and Peter H.N. de With. Catheter localization in 3d ultrasound using voxel-of-interest-based convnets for cardiac intervention. *International Journal of Computer Assisted Radiology and Surgery*, 14(6):1069–1077, 2019.

[18] Hongxu Yang, Caifeng Shan, Tao Tan, Alexander F. Kolen, and Peter H. N. de With. Transferring from ex-vivo to in-vivo: Instrument localization in 3d cardiac ultrasound using pyramid-unet with hybrid loss. In Dinggang Shen, Tianming Liu, Terry M. Peters, Lawrence H. Staib, Caroline Essert, Sean Zhou, Pew-Thian Yap, and Ali Khan, editors, *Medical Image Computing and Computer Assisted Intervention – MICCAI 2019*, pages 263–271, Cham, 2019. Springer International Publishing.

[19] R. E. Kumon, Y. Zhou, K. Yang, and C. X. Deng. Spectral analysis of ultrasound backscatter for characterization of hifu lesions in cardiac tissue high-frequency imaging. In *IEEE International Ultrasonics Symposium*, pages 244–247, 2009.

[20] Farhad Imani, Purang Abolmaesumi, Mark Z. Wu, Andras Lasso, Everette Clif Burdette, Goutam Ghoshal, Tamas Heffter, Emery Williams, Paul Neubauer, Gabor Fichtinger, and Parvin Mousavi. Ultrasound-guided characterization of interstitial ablated tissue using rf time series: Feasibility study. *IEEE Transactions on Biomedical Engineering*, 60(6):1608–1618, 2013.

[21] S. Siebers, M. Schwabe, U. Scheipers, C. Welp, J. Werner, and H. Ermert. Evaluation of ultrasonic texture and spectral parameters for coagulated tissue characterization. In *IEEE International Ultrasonics Symposium*, volume 3, pages 1804–1807, 2004.

[22] Farhad Imani, Mark Z. Wu, Andras Lasso, Everette Clif Burdette, Mohammad I. Daoud, Gabor Fitchinger, Purang Abolmaesumi, and Parvin Mousavi. Monitoring of tissue ablation using time series of ultrasound rf data. In *International Conference on Medical Image Computing and Computer-Assisted Intervention (MICCAI)*, pages 379–386, 2011.

[23] R. V. Sloun, L. Demi, C. Shan, and M. Mischi. Ultrasound coefficient of nonlinearity imaging. *IEEE Transactions on Ultrasonics, Ferroelectrics, and Frequency Control*, 62(7):1331–1341, 2015.

[24] Petia Radeva and Jasjit S Suri, editors. *Vascular and Intravascular Imaging Trends, Analysis, and Challenges, Volume 2*. 2053-2563. IOP Publishing, 2019.

[25] Mariantina Fragou, Andreas Karabinis, Eugene Daphnis, Nicolaos Labropoulos, and Dimitrios Karakitsos. Ultrasound imaging in vascular diseases. In Igor V. Minin and Oleg V. Minin, editors, *Ultrasound Imaging*, chapter 10. IntechOpen, Rijeka, 2011.

[26] D. V. Pazinato, B. V. Stein, W. R. de Almeida, R. de O. Werneck, P. R. M. Jnior, O. A. B. Penatti, R. d. S. Torres, F. H. Menezes, and A. Rocha. Pixel-level tissue classification for ultrasound images. *IEEE Journal of Biomedical and Health Informatics*, 20(1):256–267, 2016.

[27] U. Rajendra Acharya, M. M. Rama Krishnan, S. Vinitha Sree, J. Sanches, S. Shafique, A. Nicolaides, L. M. Pedro, and J. S. Suri. Plaque tissue characterization and classification in ultrasound carotid scans: A paradigm for vascular feature amalgamation. *IEEE Transactions on Instrumentation and Measurement*, 62(2):392–400, 2013.

[28] Xiaowei Huang, Yanling Zhang, Ming Qian, Long Meng, Yang Xiao, Lili Niu, Rongqin Zheng, and Hairong Zheng. Classification of carotid plaque echogenicity by combining texture features and morphologic characteristics. *Journal of Ultrasound in Medicine*, 35(10):2253–2261, 2016.

[29] S Latha, Dhanalakshmi Samiappan, and R Kumar. Carotid artery ultrasound image analysis: A review of the literature. *Proceedings of the Institution of Mechanical Engineers, Part H: Journal of Engineering in Medicine*, 234(5):417–443, 2020. PMID: 31960771.

[30] Ji-Bin Liu and BarryB Goldberg. 2-d and 3-d endoluminal ultrasound: vascular and nonvascular applications. *Ultrasound in Medicine and Biology*, 25(2):159–173, 1999.

[31] S. Sathyanarayana, S. Carlier, W. Li, and L. Thomas. Characterisation of atherosclerotic plaque by spectral similarity of radiofrequency intravascular ultrasound signals. *EuroIntervention*, 5:133–139, 2009.

[32] Sergio Escalera, Oriol Pujol, Josepa Mauri, and Petia Radeva. Intravascular ultrasound tissue characterization with sub-class error-correcting output codes. *Signal Processing Systems*, 55(1-3):35–47, 2009.

[33] Francesco Ciompi, Oriol Pujol, Carlo Gatta, Oriol Rodriguez-Leor, Josepa Mauri-Ferré, and Petia Radeva. Fusing in-vitro and in-vivo intravascular ultrasound data for plaque characterization. *International Journal of Cardiovascular Imaging*, 26(7):763–779, 2010.

[34] José C. R. Seabra, Francesco Ciompi, Oriol Pujol, Josepa Mauri, Petia Radeva, and João M. Sanches. Rayleigh mixture model for plaque characterization in intravascular ultrasound. *IEEE Transactions on Biomedical Engineering*, 58(5):1314–1324, 2011.

[35] Francesco Ciompi. *Multiclass Learning for Vessel Characterization in Intravascular Ultrasound*. PhD thesis, Universitat de Barcelona, Computer Vision Center, 2012.

[36] Juhwan Lee, Yoo Na Hwang, Ga Young Kim, Ji Yean Kwon, and Sung Min Kim. Automated classification of dense calcium tissues in gray-scale intravascular ultrasound images using a deep belief network. *BMC medical imaging*, 19(1):103, December 2019.

[37] Norman F Boyd, Helen Guo, Lisa J Martin, Limei Sun, Jennifer Stone, Eve Fishell, Roberta A Jong, Greg Hislop, Anna Chiarelli, Salomon

Minkin, et al. Mammographic density and the risk and detection of breast cancer. *New England Journal of Medicine*, 356(3):227–236, 2007.

[38] Monika Nothacker, Volker Duda, Markus Hahn, Mathias Warm, Friedrich Degenhardt, Helmut Madjar, Susanne Weinbrenner, and Ute-Susann Albert. Early detection of breast cancer: benefits and risks of supplemental breast ultrasound in asymptomatic women with mammographically dense breast tissue. a systematic review. *BMC cancer*, 9(1):335, 2009.

[39] H. D. Cheng, J. Shan, W. Ju, Y. Guo, and L. Zhang. Automated breast cancer detection and classification using ultrasound images: A survey. *Pattern Recognition*, 43(1):299–317, 2010.

[40] Wendie A Berg, Jeffrey D Blume, Jean B Cormack, Ellen B Mendelson, Daniel Lehrer, Marcela Böhm-Vélez, Etta D Pisano, Roberta A Jong, W Phil Evans, Marilyn J Morton, et al. Combined screening with ultrasound and mammography vs mammography alone in women at elevated risk of breast cancer. *Jama*, 299(18):2151–2163, 2008.

[41] Stuart S Kaplan. Clinical utility of bilateral whole-breast us in the evaluation of women with dense breast tissue. *Radiology*, 221(3):641–649, 2001.

[42] Y.-Y. Liao, P.-H. Tsui, C.-H. Li, K.-J. Chang, W.-H. Kuo, C.-C. Chang, and C.-K. Yeh. Classification of benign and malignant breast tumors by ultrasound b-scan and nakagami-based images. *Medical Physics*, 38(4):2198–2207, 2011.

[43] Jianrui Ding, H. D. Cheng, Jianhua Huang, Jiafeng Liu, and Yingtao Zhang. Breast ultrasound image classification based on multiple-instance learning. *J. Digital Imaging*, 25(5):620–627, 2012.

[44] Ahmed Sayed, Ginger Layne, Jame Abraham, and Osama M. Mukdadi. 3-d visualization and non-linear tissue classification of breast tumors using ultrasound elastography in vivo. *Ultrasound in Medicine and Biology*, 40(7):1490–1502, 2014.

[45] Tao Tan, Bram Platel, Henkjan Huisman, Clara I Sánchez, Roel Mus, and Nico Karssemeijer. Computer-aided lesion diagnosis in automated 3-d breast ultrasound using coronal spiculation. *IEEE transactions on medical imaging*, 31(5):1034–1042, 2012.

[46] Tao Tan, Bram Platel, Thorsten Twellmann, Guido van Schie, Roel Mus, André Grivegnée, Ritse M Mann, and Nico Karssemeijer. Evaluation of the effect of computer-aided classification of benign and malignant lesions on reader performance in automated three-dimensional breast ultrasound. *Academic radiology*, 20(11):1381–1388, 2013.

[47] Haixia Liu, Tao Tan, Jan van Zelst, Ritse Mann, Nico Karssemeijer, and Bram Platel. Incorporating texture features in a computer-aided breast lesion diagnosis system for automated three-dimensional breast ultrasound. *Journal of Medical Imaging*, 1(2):024501, 2014.

[48] Chiao Lo, Yi-Wei Shen, Chiun-Sheng Huang, and Ruey-Feng Chang. Computer-aided multiview tumor detection for automated whole breast ultrasound. *Ultrasonic imaging*, 36(1):3–17, 2014.

[49] Jan CM van Zelst, Maschenka Balkenhol, Tao Tan, Matthieu Rutten, Mechli Imhof-Tas, Peter Bult, Nico Karssemeijer, and Ritse M Mann. Sonographic phenotypes of molecular subtypes of invasive ductal cancer in automated 3-d breast ultrasound. *Ultrasound in medicine & biology*, 43(9):1820–1828, 2017.

[50] Tao Tan, Bram Platel, Roel Mus, Laszlo Tabar, Ritse M Mann, and Nico Karssemeijer. Computer-aided detection of cancer in automated 3-d breast ultrasound. *IEEE transactions on medical imaging*, 32(9):1698–1706, 2013.

[51] Ehsan Kozegar, Mohsen Soryani, Hamid Behnam, Masoumeh Salamati, and Tao Tan. Breast cancer detection in automated 3d breast ultrasound using iso-contours and cascaded rusboosts. *Ultrasonics*, 79:68–80, 2017.

[52] Karen Drukker, Charlene A Sennett, and Maryellen L Giger. Computerized detection of breast cancer on automated breast ultrasound imaging of women with dense breasts. *Medical physics*, 41(1), 2014.

[53] Tao Tan, Jan-Jurre Mordang, Jan van Zelst, André Grivegnée, Albert Gubern-Mérida, Jaime Melendez, Ritse M Mann, Wei Zhang, Bram Platel, and Nico Karssemeijer. Computer-aided detection of breast cancers using haar-like features in automated 3d breast ultrasound. *Medical physics*, 42(4):1498–1504, 2015.

[54] JCM Van Zelst, T Tan, B Platel, M De Jong, A Steenbakkers, M Mourits, A Grivegnee, C Borelli, N Karssemeijer, and RM Mann. Improved cancer detection in automated breast ultrasound by radiologists using computer aided detection. *European journal of radiology*, 89:54–59, 2017.

[55] Jan CM van Zelst, Tao Tan, Paola Clauser, Angels Domingo, Monique D Dorrius, Daniel Drieling, Michael Golatta, Francisca Gras, Mathijn de Jong, Ruud Pijnappel, et al. Dedicated computer-aided detection software for automated 3d breast ultrasound; an efficient tool for the radiologist in supplemental screening of women with dense breasts. *European radiology*, 28(7):2996–3006, 2018.

[56] Ehsan Kozegar, Mohsen Soryani, Hamid Behnam, M Salamati, and T Tan. Mass segmentation in automated 3-d breast ultrasound using adaptive region growing and supervised edge-based deformable model. *IEEE transactions on medical imaging*, 37(4):918–928, 2017.

[57] Ehsan Kozegar, Mohsen Soryani, Hamid Behnam, Masoumeh Salamati, and Tao Tan. Computer aided detection in automated 3-d breast ultrasound images: a survey. *Artificial Intelligence Review*, pages 1–23, 2019.

[58] `https://www.accessdata.fda.gov/cdrh_docs/pdf11/P110006B.pdf`.

[59] `https://www.accessdata.fda.gov/cdrh_docs/pdf8/K081148.pdf`.

[60] Nebojsa Duric, Peter Littrup, and CM Kuzmiak. Breast ultrasound tomography. *Breast Imaging*, 2018.

[61] Bilal H Malik and John C Klock. Breast cyst fluid analysis correlations with speed of sound using transmission ultrasound. *Academic radiology*, 26(1):76–85, 2019.

[62] Simona Maggio. *Analysis and Modeling Techniques for Ultrasonic Tissue Characterization*. PhD thesis, University of Bologna, 2011.

[63] Michael Mitterberger, Wolfgang Horninger, Friedrich Aigner, Germar M. Pinggera, Ilona Steppan, Peter Rehder, and Ferdinand Frauscher. Ultrasound of the prostate. *Cancer Imaging*, 10(1):40–48, 2010.

[64] M. Smeenge, J. J. de la Rosette, and H. Wijkstra. Current status of transrectal ultrasound techniques in prostate cancer. *Current Opinion in Urology*, 22(4):297–302, 2012.

[65] Mehdi Moradi, Parvin Mousavi, and Purang Abolmaesumi. Computer-aided diagnosis of prostate cancer with emphasis on ultrasound-based approaches: a review. *Ultrasound in Medicine and Biology*, 33(7):1010–1028, 2007.

[66] A. Huynen, R. Giesen, J. de la Rosette, R. Aarnink, F. Debruyne, and H. Wijkstra. Analysis of ultrasonographic prostate images for the detection of prostatic carcinoma: the automated urologic diagnostic expert system. *Ultrasound in Medicine and Biology*, 20(1):1–10, 1994.

[67] U. Scheipers, H. Ermert, H. J. Sommerfeld, M. Garcia-Schurmann, T. Senge, and S. Philippou. Ultrasonic multifeature tissue characterization for prostate diagnostics. *Ultrasound in Medicine and Biology*, 29(8):1137–1149, 2003.

[68] S. S. Mohamed and Magdy M. A. Salama. Prostate cancer spectral multifeature analysis using trus images. *IEEE Transactions on Medical Imaging*, 27(4):548–556, 2008.

[69] Seok Min Han, Hak Jong Lee, and Jin Young Choi. Computer-aided prostate cancer detection using texture features and clinical features in ultrasound image. *Journal of Digital Imaging*, 21(Suppl 1):S121–S133, 2008.

[70] Gyan Pareek, U. Rajendra Acharya, S. Vinitha Sree, G. Swapna, Ratna Yantri, Roshan Joy Martis, Luca Saba, Ganapathy Krishnamurthi, Giorgio Mallarini, Ayman El-Baz, Shadi Al Ekish, Michael Beland, and Jasjit S. Suri. Prostate tissue characterization/classification in 144 patient population using wavelet and higher order spectra features from transrectal ultrasound images. *Technology in Cancer Research & Treatment*, 12(6):545–557, 2013. PMID: 23745787.

[71] J. Braeckman, P. Autier, C. Garbar, M. P. Marichal, C. Soviany, R. Nir, D. Nir, D. Michielsen, H. Bleiberg, L. Egevad, and M. Emberton. Computer-aided ultrasonography (histoscanning): a novel technology for locating and characterizing prostate cancer. *BJU International*, 101(3):293–298, 2008.

[72] Lucy A.M. Simmons, Philippe Autier, Frantiek Zt'ura, Johan Braeckman, Alexandre Peltier, Imre Romic, Arnulf Stenzl, Karien Treurnicht, Tara Walker, Dror Nir, Caroline M. Moore, and Mark Emberton. Detection, localisation and characterisation of prostate cancer by prostate histoscanning. *BJU International*, 110(1):28–35, 2012.

[73] James S. Wysock, Alex Xu, Clement Orczyk, and Samir S. Taneja. Histoscanningtm to detect and characterize prostate cancera review of existing literature. *Current Urology Reports*, 18, 2017.

[74] Frank K. Chen, Andre Luis de Castro Abreu, and Suzanne L. Palmer. Utility of ultrasound in the diagnosis, treatment, and follow-up of prostate cancer: State of the art. *The Journal of Nuclear Medicine*, 57, 2016.

[75] J.-M. Correas, A.-M. Tissier, A. Khairoune, G. Khoury, D. Eiss, and O. Helenon. Ultrasound elastography of the prostate: State of the art. *Diagnostic and Interventional Imaging*, 94(5):551–560, 2013.

[76] Joy Liau, Daniel Goldberg, and Hina Arif-Tiwari. Prostate cancer detection and diagnosis: Role of ultrasound with mri correlates. *Current Radiology Reports*, 7, 2019.

[77] Guangming Xian. An identification method of malignant and benign liver tumors from ultrasonography based on glcm texture features and fuzzy svm. *Expert Syst. Appl.*, 37(10):6737–6741, 2010.

[78] Wen-Li Lee and Kai-Sheng Hsieh. A robust algorithm for the fractal dimension of images and its applications to the classification of natural images and ultrasonic liver images. *Signal Processing*, 90(6):1894–1904, 2010.

[79] Wen-Li Lee. Ultrasonic liver tissue characterization by multiresolution feature vector and an ensemble of classifiers. *International Journal of Innovative Computing, Information and Control*, 7(11):6541–6558, 2011.

[80] Jaehyun Jeon, Jae Young Choi, Sihyoung Lee, and Yong Man Ro. Multiple roi selection based focal liver lesion classification in ultrasound images. *Expert Syst. Appl.*, 40(2):450–457, 2013.

[81] S. J. Chen, S. N. Yu, J. E. Tzeng, Y. T. Chen, K. Y. Chang, K. S. Cheng, F. T. Hsiao, and C. K. Wei. Characterization of the major histopathological components of thyroid nodules using sonographic textural features for clinical diagnosis and management. *Ultrasound in Medicine and Biology*, 35(2):201–8, 2009.

[82] J. Ding, H. Cheng, C. Ning, J. Huang, and Y. Zhang. Quantitative measurement for thyroid cancer characterization based on elastography. *J. Ultrasound Med.*, 30(9):1259–66, 2011.

[83] U. R. Acharya, O. Faust, S. V. Sree, F. Molinari, and J. S. Suri. Thyroscreen system: High resolution ultrasound thyroid image characterization into benign and malignant classes using novel combination of texture and discrete wavelet transform. *Computer Methods and Programs in Biomedicine*, 107(2):233–41, 2012.

[84] U. R. Acharya, G. Swapna, S. Vinitha Sree, Filippo Molinari, Savita Gupta, Ricardo H. Bardales, Agnieszka Witkowska, and Jasjit S. Suri. A review on ultrasound-based thyroid cancer tissue characterization and automated classification. *Technology in Cancer Research and Treatment*, 13(4):289–301, 2014.

[85] Oriol Pujol, Misael Rosales, Petia Radeva, and Eduard Fernández-Nofrerías. Intravascular ultrasound images vessel characterization using adaboost. In *International Conference on Functional Imaging and Modeling of the Heart (FIMH)*, pages 242–251, 2003.

[86] W. C. Yeh, Y. M. Jeng, C. H. Li, P. H. Lee, and P. C. Li. Liver steatosis classification using high-frequency ultrasound. *Ultrasound in Medicine and Biology*, 31(5):599–605, 2005.

[87] Karla L. Caballero, Joel Barajas, Oriol Pujol, Oriol Rodriguez, and Petia Radeva. Using reconstructed ivus images for coronary plaque classification. In *Annual International Conference of the IEEE Engineering in Medicine and Biology Society (EMBS)*, pages 2167–2170, 2007.

[88] Mehdi Moradi, Purang Mousavi, Alexander Boag, Eric Sauerbrei, Robert Siemens, and Purang Abolmaesumi. Augmenting detection of prostate cancer in transrectal ultrasound images using svm and rf time series. *IEEE Transactions on Biomedical Engineering*, 56(9):2214–2224, 2009.

[89] Ming-Huwi Horng. Multi-class support vector machine for classification of the ultrasonic images of supraspinatus. *Expert Syst. Appl.*, 36(4):8124–8133, 2009.

[90] Simona Maggio, Alessandro Palladini, Luca De Marchi, Martino Alessandrini, Nicolo Speciale, and Guido Masetti. Predictive deconvolution and hybrid feature selection for computer-aided detection of prostate cancer. *IEEE Transactions on Medical Imaging*, 29(2):455–464, 2010.

[91] D. Glotsos, I. Kalatzis, P. Theocharakis, P. Georgiadis, A. Daskalakis, K. Ninos, P. Zoumboulis, A. Filippidou, and D. Cavouras. A multiclassifier system for the characterization of normal, infectious, and cancerous prostate tissues employing transrectal ultrasound images. *Computer Methods and Programs in Biomedicine*, 97(1):53–61, 2010.

[92] Bo Liu, H.D. Cheng, Jianhua Huang, Jiawei Tian, Xianglong Tang, and Jiafeng Liu. Fully automatic and segmentation-robust classification of breast tumors based on local texture analysis of ultrasound images. *Pattern Recognition*, 43(1):280–298, 2010.

[93] Woo Kyung Moon, Yi-Wei Shen, Chiun-Sheng Huang, Li-Ren Chiang, and Ruey-Feng Chang. Computer-aided diagnosis for the classification of breast masses in automated whole breast ultrasound images. *Ultrasound in Medicine and Biology*, 37(4):539–548, 2011.

[94] U. R. Acharya, S. V. Sree, R. Ribeiro, G. Krishnamurthi, R. T. Marinho, J. Sanches J, and J. S. Suri. Data mining framework for fatty liver disease classification in ultrasound: a hybrid feature extraction paradigm. *Medical Physics*, 39(7):4255–64, 2012.

[95] Vasilis G. Giannoglou, Dimitris G. Stavrakoudis, John B. Theocharis, and Vasilios Petridis. Genetic fuzzy rule based classification systems for coronary plaque characterization based on intravascular ultrasound images. *Engineering Applications of Artificial Intelligence*, 38:203–220, 2015.

[96] Francesco Ciompi, Oriol Pujol, Oriol Rodriguez-Leor, Carlo Gatta, Angel Serrano Vida, and Petia Radeva. Enhancing in-vitro ivus data for tissue characterization. In *4th Iberian Conference on Pattern Recognition and Image Analysis*, pages 241–248, 2009.

[97] Wen-Li Lee, Yung-Chang Chen, and Kai-Sheng Hsieh. Ultrasonic liver tissues classification by fractal feature vector based on m-band wavelet transform. *IEEE Transactions on Medical Imaging*, 22(3):382–392, 2003.

[98] R. Ribeiro and J. Sanches. Fatty liver characterization and classification by ultrasound. In *Iberian Conference on Pattern Recognition and Image Analysis*, pages 354–361, 2009.

[99] J. Wan and S. Zhou. Features extraction based on wavelet packet transform for b-mode ultrasound liver images. In *International Congress on Image and Signal Processing*, pages 949–955, 2010.

[100] Y.-Y. Liao, P.-H. Tsui, and C.-K. Yeh. Classification of scattering media within benign and malignant breast tumors based on ultrasound texture-feature-based and kakagami-parameter images. *Journal of Medical and Biological Engineering*, 30(5):307–312, 2010.

[101] P.-H. Tsui, Y.-Y. Liao, C.-C. Chang, W.-H. Kuo, K.-J. Chang, and C.-K. Yeh. Classification of benign and malignant breast tumors by 2-d analysis based on contour description and scatterer characterization. *IEEE Transactions on Medical Imaging*, 29(2):513–22, 2010.

[102] Tao Tan, Jan-Jurre Mordang, Jan Zelst, André Grivegnée, Albert Gubern-Mérida, Jaime Melendez, Ritse M Mann, Wei Zhang, Bram Platel, and Nico Karssemeijer. Computer-aided detection of breast cancers using haar-like features in automated 3d breast ultrasound. *Medical physics*, 42(4):1498–1504, 2015.

[103] F. L. Lizzi, M. Greenebaum, E. J. Feleppa, M. Elbaum, and D. J. Coleman. Theoretical framework for spectrum analysis in ultrasonic tissue characterization. *J. Acoust. Soc. Amer.*, 73(4):1366–1373, 1983.

[104] Anuja Nair, Barry D. Kuban, N. Obuchowski, and D. G. Vince. Assessing spectral algorithms to predict atherosclerotic plaque composition with normalized and raw intravascular ultrasound data. *Ultrasound in Medicine and Biology*, 27(1):1319–1331, 2001.

[105] A. Nair, B. D. Kuban, E. M. Tuzcu, P. Schoenhagen, S. E. Nissen, and D. G. Vince. Coronary plaque classification with intravascular ultrasound radiofrequency data analysis. *Circulation*, 106(17):2200–2206, 2002.

[106] E. J. Feleppa, C. R. Porter, J. Ketterling, P. Lee, S. Dasgupta, S. Urban, and A. Kalisz. Recent developments in tissue-type imaging (tti) for planning and monitoring treatment of prostate cancer. *Ultrasonic Imaging*, 26(3):163–72, 2004.

[107] Amin Katouzian, S. Sathyanarayana, Babak Baseri, Elisa E. Konofagou, and Stephane G. Carlier. Challenges in atherosclerotic plaque characterization with intravascular ultrasound (ivus): From data collection to classification. *IEEE Transactions on Information Technology in Biomedicine*, 12(3):315–327, 2008.

[108] Ernest J. Feleppa, Mark J. Rondeau, Paul Lee, and Christopher R. Porter. Prostate-cancer imaging using machine-learning classifiers: Potential value for guiding biopsies, targeting therapy, and monitoring treatment. In *IEEE International Ultrasonics Symposium*, pages 527–529, 2009.

[109] T. Liu, M. M. Mansukhani, M. C. Benson, R. Ennis, E. Yoshida, P. B. Schiff, P. Zhang, J. Zhou, and G. J. Kutcher. A feasibility study of novel ultrasonic tissue characterization for prostate-cancer diagnosis: 2d spectrum analysis of in vivo data with histology as gold standard. *Medical Physics*, 36(8):3504–11, 2009.

[110] Mehdi Moradi, Christian Wachinger, Andriy Fedorov, William M. Wells, Tina Kapur, Luciant D. Wolfsberger, Paul Nguyen, and Clare M. Tempany. Mri confirmed prostate tissue classification with laplacian eigenmaps of ultrasound rf spectra. In *Third International Workshop on Machine Learning in Medical Imaging*, pages 19–26, 2012.

[111] Hai Li, Patrick D. Kumavor, Umar Alqasemi, and Quing Zhu. Classification algorithm of ovarian tissue based on co-registered ultrasound and photoacoustic tomography. In *Proc. SPIE 8943, Photons Plus Ultrasound: Imaging and Sensing*, 2014.

[112] M. Moradi, P. Mousavi, D. R. Siemens, E. E. Sauerbrei, P. Isotalo, A. Boag, and P. Abolmaesumi. Discrete fourier analysis of ultrasound rf time series for detection of prostate cancer. In *Annual International Conference of the IEEE Engineering in Medicine and Biology Society (EMBS)*, pages 1339–42, 2007.

[113] Mehdi Moradi, Parvin Mousavi, and Purang Abolmaesumi. Tissue characterization using fractal dimension of high frequency ultrasound rf time series. In *International Conference on Medical Image Computing and Computer-Assisted Intervention (MICCAI)*, pages 900–908, 2007.

[114] M. Moradi, P. Abolmaesumi, and P. Mousavi. Tissue typing using ultrasound rf time series: Experiments with animal tissue samples. *Medical Physics*, 37(8):4401–13, 2010.

[115] Farhad Imani, Mohammad I. Daoud, Mehdi Moradi, Purang Abolmaesumi, and Parvin Mousavi. Tissue classification using depth-dependent ultrasound time series analysis: in-vitro animal study. In *SPIE Medical Imaging*, page 79860F, 2011.

[116] M. Moradi, S. Sara Mahdavi, Guy Nir, Edward C. Jones, S. Larry Goldenberg, and Septimiu E. Salcudean. Ultrasound rf time series for tissue typing: First in vivo clinical results. In *SPIE Medical Imaging*, 2013.

[117] Nishant Uniyal, Farhad Imani, Amir Tahmasebi, Peter Choyke, Baris Turkbey, Peter Pinto, Bradford Wood, Sheng Xu, Jin Tae Kwak, Pingkun Yan, Jochen Kruecker, Shyam Bharat, Harsh Agarwal, Purang Abolmaesumi, Parvin Mousavi, and Mehdi Moradi. Ultrasound-based predication of prostate cancer in mri-guided biopsy. In *The 3rd MICCAI Workshop on Clinical Image-based Procedures: Translational Research in Medical Imaging*, 2014.

[118] Amir Khojaste, Farhad Imani, Mehdi Moradi, David Berman, D. Robert Siemens, Eric E. Sauerberi, Alexander H. Boag, Purang Abolmaesumi, and Parvin Mousavi. Characterization of aggressive prostate cancer using ultrasound RF time series. In Lubomir M. Hadjiiski and Georgia D. Tourassi, editors, *Medical Imaging 2015: Computer-Aided Diagnosis*, volume 9414, pages 326 – 333. International Society for Optics and Photonics, SPIE, 2015.

[119] D. Sheet, A. Karamalis, N. Navab, A. F. Laine, J. Chatterjee, A. K. Ray, S. G. Carlier, and A. Katouzian. Machine learning of ultrasonic statistical physics primal for tissue characterization in intravascular ultrasound. In *Annual International Conference of the IEEE Engineering in Medicine and Biology Society (EMBC)*, 2012.

[120] M. Aboofazeli, P. Abolmaesumi, G. Fichtinger, and P. Mousavi. Tissue characterization using multiscale products of wavelet transform of ultrasound radio frequency echoes. In *Annual International Conference of the IEEE Engineering in Medicine and Biology Society (EMBS)*, pages 479–482, 2009.

[121] Oliver Faust, U. Rajendra Acharya, Kristen M.Meiburger, Filippo Molinari, Joel E.W.Koh, Chai Hong Yeong, Pailin Kongmebhol, and Kwan Hoong Ng. Comparative assessment of texture features for the identification of cancer in ultrasound images: a review. *Biocybernetics and Biomedical Engineering*, 38(2):275–296, 2018.

[122] Robert M Haralick, K Shanmugam, and Itsḥak Dinstein. Textural features for image classification. *IEEE Transactions on Systems, Man and Cybernetics*, SMC-3:610–621, 1973.

[123] J. G. Daugman. Complete discrete 2d gabor transform by neural networks for image analysis and compression. *IEEE Trans. Acoustics, Speech, and Signal Processing*, 36(7):1169–1179, July 1988.

[124] T. Ojala, M. Pietikäinen, and T. Mäenpää. Multiresolution gray-scale and rotation invariant texture classification with local binary patterns. *IEEE Transactions on Pattern Analysis and Machine Intelligence*, 24(7):971–987, 2002.

[125] Mihran Tuceryan. Moment-based texture segmentation. *Pattern Recognition Letters*, 15(7):659–668, 1994.

[126] Karla L. Caballero, Joel Barajas, Oriol Pujol, Neus Salvatella, and Petia Radeva. In-vivo ivus tissue classification: A comparison between rf signal analysis and reconstructed images. In *Progress in Pattern Recognition, Image Analysis and Applications, 11th Iberoamerican Congress in Pattern Recognition (CIARP)*, pages 137–146, 2006.

[127] Michael Unser. Sum and difference histograms for texture classification. *IEEE Trans. Pattern Anal. Mach. Intell.*, 8(1):118–125, 1986.

[128] U. R. Acharya, Oliver Faust, Filippo Molinari, S. Vinitha Sree, Junnarkar Sameer Padmakumar, and S. Vidya. Ultrasound-based tissue characterization and classification of fatty liver disease: A screening and diagnostic paradigm. *Knowledge-Based Systems*, 75:66–77, 2015.

[129] R. F. Wagner, S. W. Smith, J. M. Sandrik, and H. Lopez. Statistics of speckle in ultrasound b-scans. *IEEE Transactions on Sonics and Ultrasonics*, 30(3):156–163, 1983.

[130] F. L. Lizzi, M. Ostromogilsky, E. J. Feleppa, M. C. Rorke, and M. M. Yaremko. Relationship of ultrasonic spectral parameters to features of tissue microstructure. *IEEE Transactions on Ultrasonics, Ferroelectrics and Frequency Control*, 34(3):319–329, 1987.

[131] T. Liu, F. L. Lizzi, J. A. Ketterling, R. H. Silverman, and G. J. Kutcher. Ultrasonic tissue characterization via 2-d spectrum analysis: Theory and in vitro measurements. *Medical Physics*, 34(3):1037–46, 2007.

[132] Mohammad I. Daoud, Parvin Mousavi, Farhad Imani, Robert Rohling, and Purang Abolmaesumi. Computer-aided tissue characterization using ultrasound-induced thermal effects: Analytical formulation and in-vitro animal study. In *Proc. SPIE 7968, Medical Imaging*, 2011.

[133] Mohammad I. Daoud, Parvin Mousavi, Farhad Imani, Robert Rohling, and Purang Abolmaesumi. Tissue classification using ultrasound-induced variations in acoustic backscattering features. *IEEE Transactions on Biomedical Engineering*, 60(2):310–320, 2013.

[134] Francois Destrempes and Guy Cloutier. A critical review and uniformized representation of statistical distributions modeling the ultrasound echo envelope. *Ultrasound in Medicine and Biology*, 36(7):1037–1051, 2010.

[135] José C. R. Seabra, Francesco Ciompi, Petia Radeva, and João M. Sanches. *Ultrasound Imaging: Advances and Applications*, chapter A Rayleigh Mixture Model for IVUS Imaging, pages 25–47. Springer, 2012.

[136] Si Luo, Eung-Hun Kim, Manjiri Dighe, and Yongmin Kim. Thyroid nodule classification using ultrasound elastography via linear discriminant analysis. *Ultrasonics*, 51(4):425–431, 2011.

[137] Ryosuke Kubota, Mami Kunihiro, Noriaki Suetake, Eiji Uchino, Genta Hashimoto, Takafumi Hiro, and Masunori Matsuzaki. An intravascular ultrasound-based tissue characterization using shift-invariant features extracted by adaptive subspace som. *International Journal of Biology and Biomedical Engineering*, 2(2):79–88, 2008.

[138] Victor S. Lempitsky, Michael Verhoek, J. Alison Noble, and Andrew Blake. Random forest classification for automatic delineation of myocardium in real-time 3d echocardiography. In *International Conference on Functional Imaging and Modeling of the Heart (FIMH)*, pages 447–456, 2009.

[139] Debdoot Sheet, Athanasios Karamalis, Abouzar Eslami, Peter Noel, Jyotirmoy Chatterjee, Ajoy K. Ray, Andrew F. Laine, Stephane G. Carlier, Nassir Navab, and Amin Katouzian. Joint learning of ultrasonic backscattering statistical physics and signal confidence primal for characterizing atherosclerotic plaques using intravascular ultrasound. *Medical Image Analysis*, 18(1):103–117, 2014.

[140] P. N. Belhumeur, J. P. Hespanha, and D. J. Kriegman. Eigenfaces vs. fisherfaces: Recognition using class specific linear projection. *IEEE Transactions on Pattern Analysis and Machine Intelligence*, 19(7):711–720, July 1997.

[141] V. N. Vapnik. *Statistical Learning Theory*. Wiley, New York, 1998.

[142] Y. Freund and R. E. Schapire. A decision-theoretic generalization of on-line learning and an application to boosting. *Journal of Computer and System Sciences*, 55(1):119–139, 1997.

[143] L. Breiman. Random forests. *Machine Learning*, 45(1):5–32, 2001.

[144] Erin L. Allwein, Robert E. Schapire, and Yoram Singer. Reducing multiclass to binary: A unifying approach for margin classifiers. *Journal of Machine Learning Research*, 1:113–141, 2000.

[145] Oriol Pujol and David Masip. Geometry-based ensembles: Toward a structural characterization of the classification boundary. *IEEE Trans. Pattern Anal. Mach. Intell.*, 31(6):1140–1146, 2009.

[146] Shengfeng Liu, Yi Wang, Xin Yang, Baiying Lei, Li Liu, Shawn Xiang Li, Dong Ni, and Tianfu Wang. Deep learning in medical ultrasound analysis: a review. *Engineering*, 2019.

[147] Geert Litjens, Thijs Kooi, Babak Ehteshami Bejnordi, Arnaud Arindra Adiyoso Setio, Francesco Ciompi, Mohsen Ghafoorian, Jeroen Awm Van Der Laak, Bram Van Ginneken, and Clara I Sánchez. A survey on deep learning in medical image analysis. *Medical image analysis*, 42:60–88, 2017.

[148] Alex Krizhevsky, Ilya Sutskever, and Geoffrey E. Hinton. Imagenet classification with deep convolutional neural networks. *Commun. ACM*, 60(6):84–90, May 2017.

[149] Kaiming He, Xiangyu Zhang, Shaoqing Ren, and Jian Sun. Deep residual learning for image recognition. In *Computer Vision and Pattern Recognition*, pages 770–778, 2016.

[150] Gao Huang, Zhuang Liu, Kilian Q Weinberger, and Laurens van der Maaten. Densely connected convolutional networks. *arXiv preprint arXiv:1608.06993*, 2016.

[151] Olaf Ronneberger, Philipp Fischer, and Thomas Brox. U-net: Convolutional networks for biomedical image segmentation. In *International Conference on Medical image computing and computer-assisted intervention*, pages 234–241. Springer, 2015.

[152] Kaizhi Wu, Xi Chen, and Mingyue Ding. Deep learning based classification of focal liver lesions with contrast-enhanced ultrasound. *Optik-International Journal for Light and Electron Optics*, 125(15):4057–4063, 2014.

[153] Gustavo Carneiro, Jacinto C Nascimento, and António Freitas. The segmentation of the left ventricle of the heart from ultrasound data using deep learning architectures and derivative-based search methods. *IEEE Transactions on Image Processing*, 21(3):968–982, 2012.

[154] E. Smistad, A. Ostvik, B. O. Haugen, and L. Lovstakken. 2D left ventricle segmentation using deep learning. In *Proc. IEEE Int. Ultrasonics Symp. (IUS)*, pages 1–4, September 2017.

[155] K. Lekadir, A. Galimzianova, Angels. Betriu, M. del Mar Vila, L. Igual, D. L. Rubin, E. Fernandez, P. Radeva, and S. Napel. A convolutional neural network for automatic characterization of plaque composition in carotid ultrasound. *IEEE Journal of Biomedical and Health Informatics*, 21(1):48–55, January 2017.

[156] Y. Feng, F. Yang, X. Zhou, Y. Guo, F. Tang, F. Ren, J. Guo, and S. Ji. A deep learning approach for targeted contrast-enhanced ultrasound based prostate cancer detection. *IEEE/ACM Transactions on Computational Biology and Bioinformatics*, page 1, 2018.

[157] J. Jang, Y. Park, B. Kim, S. M. Lee, J. Y. Kwon, and J. K. Seo. Automatic estimation of fetal abdominal circumference from ultrasound images. *IEEE Journal of Biomedical and Health Informatics*, page 1, 2017.

[158] Arijit Patra and J Alison Noble. Hierarchical class incremental learning of anatomical structures in fetal echocardiography videos. *IEEE Journal of Biomedical and Health Informatics*, 2020.

[159] Y. Zhu, Z. Fu, and J. Fei. An image augmentation method using convolutional network for thyroid nodule classification by transfer learning. In *Proc. 3rd IEEE Int. Conf. Computer and Communications (ICCC)*, pages 1819–1823, December 2017.

[160] H. Ravishankar, S. M. Prabhu, V. Vaidya, and N. Singhal. Hybrid approach for automatic segmentation of fetal abdomen from ultrasound images using deep learning. In *Proc. IEEE 13th Int. Symp. Biomedical Imaging (ISBI)*, pages 779–782, April 2016.

[161] V. Zyuzin, P. Sergey, A. Mukhtarov, T. Chumarnaya, O. Solovyova, A. Bobkova, and V. Myasnikov. Identification of the left ventricle endocardial border on two-dimensional ultrasound images using the convolutional neural network unet. In *Proc. Radioelectronics and Information Technology (USBEREIT) 2018 Ural Symp. Biomedical Engineering*, pages 76–78, May 2018.

[162] S. I. Jabbar, C. R. Day, N. Heinz, and E. K. Chadwick. Using convolutional neural network for edge detection in musculoskeletal ultrasound images. In *Proc. Int. Joint Conf. Neural Networks (IJCNN)*, pages 4619–4626, July 2016.

[163] D. Mishra, S. Chaudhury, M. Sarkar, S. Manohar, and A. S. Soin. Segmentation of vascular regions in ultrasound images: A deep learning approach. In *Proc. IEEE Int. Symp. Circuits and Systems (ISCAS)*, pages 1–5, May 2018.

[164] Yizhe Zhang, Michael TC Ying, Lin Yang, Anil T Ahuja, and Danny Z Chen. Coarse-to-fine stacked fully convolutional nets for lymph node segmentation in ultrasound images. In *Bioinformatics and Biomedicine (BIBM), 2016 IEEE International Conference on*, pages 443–448. IEEE, 2016.

[165] Moi Hoon Yap, Gerard Pons, Joan Martí, Sergi Ganau, Melcior Sentís, Reyer Zwiggelaar, Adrian K Davison, and Robert Martí. Automated breast ultrasound lesions detection using convolutional neural networks. *IEEE journal of biomedical and health informatics*, 2017.

[166] Hariharan Ravishankar, S Thiruvenkadam, R Venkataramani, and V Vaidya. Joint deep learning of foreground, background and shape for robust contextual segmentation. In *International Conference on Information Processing in Medical Imaging*, pages 622–632. Springer, 2017.

[167] Lingyun Wu, Yang Xin, Shengli Li, Tianfu Wang, Pheng-Ann Heng, and Dong Ni. Cascaded fully convolutional networks for automatic prenatal ultrasound image segmentation. In *Biomedical Imaging (ISBI 2017), 2017 IEEE 14th International Symposium on*, pages 663–666. IEEE, 2017.

[168] Ozan Oktay, Enzo Ferrante, Konstantinos Kamnitsas, Mattias Heinrich, Wenjia Bai, Jose Caballero, Stuart A Cook, Antonio de Marvao, Timothy Dawes, Declan P ORegan, et al. Anatomically constrained neural networks (acnns): application to cardiac image enhancement and segmentation. *IEEE transactions on medical imaging*, 37(2):384–395, 2018.

[169] Fausto Milletari, Seyed-Ahmad Ahmadi, Christine Kroll, Annika Plate, Verena Rozanski, Juliana Maiostre, Johannes Levin, Olaf Dietrich, Birgit Ertl-Wagner, Kai Botzel, and Nassir Navab. Hough-CNN: Deep learning for segmentation of deep brain regions in MRI and ultrasound. *Computer Vision and Image Understanding*, 164:92–102, November 2017.

[170] V. Sundaresan, C. P. Bridge, C. Ioannou, and J. A. Noble. Automated characterization of the fetal heart in ultrasound images using fully convolutional neural networks. In *Proc. IEEE 14th Int. Symp. Biomedical Imaging (ISBI 2017)*, pages 671–674, April 2017.

[171] L. Wu, Y. Xin, S. Li, T. Wang, P. A. Heng, and D. Ni. Cascaded fully convolutional networks for automatic prenatal ultrasound image segmentation. In *Proc. IEEE 14th Int. Symp. Biomedical Imaging (ISBI 2017)*, pages 663–666, April 2017.

[172] Yi Wang, Na Wang, Min Xu, Junxiong Yu, Chenchen Qin, Xiao Luo, Xin Yang, Tianfu Wang, Anhua Li, and Dong Ni. Deeply-supervised networks with threshold loss for cancer detection in automated breast ultrasound. *IEEE transactions on medical imaging*, 2019.

[173] T. Chiang, Y. Huang, R. Chen, C. Huang, and R. Chang. Tumor detection in automated breast ultrasound using 3-d cnn and prioritized candidate aggregation. *IEEE Transactions on Medical Imaging*, 38(1):240–249, 2019.

[174] Carl Azzopardi, Kenneth Camilleri, and Yulia Alexandrovna Hicks. Bimodal automated carotid ultrasound segmentation using geometrically constrained deep neural networks. *IEEE Journal of Biomedical and Health Informatics*, 2020.

[175] Erlei Zhang, Stephen Seiler, Mingli Chen, Weiguo Lu, and Xuejun Gu. Birads features-oriented semi-supervised deep learning for breast ultrasound computer-aided diagnosis. *Physics in Medicine & Biology*, 2020.

[176] Tomoyuki Fujioka, Kazunori Kubota, Mio Mori, Yuka Kikuchi, Leona Katsuta, Mai Kasahara, Goshi Oda, Toshiyuki Ishiba, Tsuyoshi Nakagawa, and Ukihide Tateishi. Distinction between benign and malignant breast masses at breast ultrasound using deep learning method with convolutional neural network. *Japanese journal of radiology*, 37(6):466–472, 2019.

[177] Wen-Xuan Liao, Ping He, Jin Hao, Xuan-Yu Wang, Ruo-Lin Yang, Dong An, and Li-Gang Cui. Automatic identification of breast ultrasound image based on supervised block-based region segmentation algorithm and features combination migration deep learning model. *IEEE Journal of Biomedical and Health Informatics*, 2019.

[178] J. Xing, Z. Li, B. Wang, Y. Qi, B. Yu, F. G. Zanjani, A. Zheng, R. Duits, and T. Tan. Lesion segmentation in ultrasound using semi-pixel-wise cycle generative adversarial nets. *IEEE/ACM Transactions on Computational Biology and Bioinformatics*, pages 1–1, 2020.

[179] Børge Solli Andreassen, Federico Veronesi, Olivier Gerard, Anne H Schistad Solberg, and Eigil Samset. Mitral annulus segmentation using deep learning in 3d transesophageal echocardiography. *IEEE Journal of Biomedical and Health Informatics*, 2019.

[180] H. Ravishankar, R. Venkataramani, S. Thiruvenkadam, P. Sudhakar, and V. Vaidya. Learning and Incorporating Shape Models for Semantic Segmentation. In *Medical Image Computing and Computer Assisted Intervention MICCAI 2017*, Lecture Notes in Computer Science, pages 203–211. Springer, Cham, September 2017.

[181] T. Liu, S. Xie, J. Yu, L. Niu, and W. Sun. Classification of thyroid nodules in ultrasound images using deep model based transfer learning and hybrid features. In *Proc. Speech and Signal Processing (ICASSP) 2017 IEEE Int. Conf. Acoustics*, pages 919–923, March 2017.

[182] Sinno Jialin Pan and Qiang Yang. A survey on transfer learning. *IEEE Transactions on knowledge and data engineering*, 22(10):1345–1359, 2010.

[183] Jason Yosinski, Jeff Clune, Yoshua Bengio, and Hod Lipson. How transferable are features in deep neural networks? *Eprint Arxiv*, 27:3320–3328, 2014.

[184] Hao Chen, Dong Ni, Jing Qin, Shengli Li, Xin Yang, Tianfu Wang, and Pheng Ann Heng. Standard plane localization in fetal ultrasound via domain transferred deep neural networks. *IEEE journal of biomedical and health informatics*, 19(5):1627–1636, 2015.

[185] Hao Chen, Qi Dou, Dong Ni, Jie-Zhi Cheng, Jing Qin, Shengli Li, and Pheng-Ann Heng. Automatic Fetal Ultrasound Standard Plane Detection Using Knowledge Transferred Recurrent Neural Networks. In *Medical Image Computing and Computer-Assisted Intervention – MICCAI 2015*, Lecture Notes in Computer Science, pages 507–514. Springer, Cham, October 2015.

[186] H. Li, J. Fang, S. Liu, X. Liang, X. Yang, Z. Mai, M. T. Van, T. Wang, Z. Chen, and D. Ni. Cr-unet: A composite network for ovary and follicle segmentation in ultrasound images. *IEEE Journal of Biomedical and Health Informatics*, 24(4):974–983, 2020.

[187] Shekoofeh Azizi, Sharareh Bayat, Pingkun Yan, Amir Tahmasebi, Guy Nir, Jin Tae Kwak, Sheng Xu, Storey Wilson, Kenneth A. Iczkowski, M. Scott Lucia, Larry Goldenberg, Septimiu E. Salcudean, Peter A. Pinto, Bradford Wood, Purang Abolmaesumi, and Parvin Mousavi. Detection and grading of prostate cancer using temporal enhanced ultrasound: combining deep neural networks and tissue mimicking simulations. *International Journal of Computer Assisted Radiology and Surgery*, 12(8):1293–1305, August 2017.

[188] M. H. Yap, G. Pons, J. Marti, S. Ganau, M. Sentis, R. Zwiggelaar, A. K. Davison, and R. Marti. Automated breast ultrasound lesions detection using convolutional neural networks. *IEEE Journal of Biomedical and Health Informatics*, 22(4):1218–1226, July 2018.

[189] Ji-kui Liu, Hong-yang Jiang, Chen-guang He, Yu Wang, Pu Wang, He Ma, et al. An assisted diagnosis system for detection of early pulmonary nodule in computed tomography images. *Journal of medical systems*, 41(2):30, 2017.

[190] Jianning Chi, Ekta Walia, Paul Babyn, Jimmy Wang, Gary Groot, and Mark Eramian. Thyroid nodule classification in ultrasound images by fine-tuning deep convolutional neural network. *Journal of Digital Imaging*, 30(4):477, August 2017.

[191] D. Meng, L. Zhang, G. Cao, W. Cao, G. Zhang, and B. Hu. Liver fibrosis classification based on transfer learning and fcnet for ultrasound images. *IEEE Access*, 5:5804–5810, 2017.

[192] Hongxu Yang, Caifeng Shan, Tao Tan, Alexander F Kolen, et al. Transferring from ex-vivo to in-vivo: Instrument localization in 3d cardiac ultrasound using pyramid-unet with hybrid loss. In *International Conference on Medical Image Computing and Computer-Assisted Intervention*, pages 263–271. Springer, 2019.

[193] Nora Baka, Sieger Leenstra, and Theo van Walsum. Ultrasound aided vertebral level localization for lumbar surgery. *IEEE transactions on medical imaging*, 36(10):2138–2147, 2017.

[194] Phillip M. Cheng and Harshawn S. Malhi. Transfer Learning with Convolutional Neural Networks for Classification of Abdominal Ultrasound Images. *Journal of Digital Imaging*, 30(2):234–243, April 2017.

[195] David Zipser Ronald J. Williams. A learning algorithm for continually running fully recurrent neural networks, 1989.

[196] Felix A. Gers, Nicol N. Schraudolph, and Jurgen Schmidthuber. Learning precise timing with lstm recurrent networks, 2002.

[197] Inan Guler and Elif Derya Ubeyli. A recurrent neural network classifier for Doppler ultrasound blood flow signals. *Pattern Recognition Letters*, 27(13):1560–1571, October 2006.

[198] S. Azizi, S. Bayat, P. Yan, A. Tahmasebi, J. T. Kwak, S. Xu, B. Turkbey, P. Choyke, P. Pinto, B. Wood, P. Mousavi, and P. Abolmaesumi. Deep Recurrent Neural Networks for Prostate Cancer Detection: Analysis of Temporal Enhanced Ultrasound. *IEEE Transactions on Medical Imaging*, pages 1–1, 2018.

[199] H. Chen, L. Wu, Q. Dou, J. Qin, S. Li, J. Z. Cheng, D. Ni, and P. A. Heng. Ultrasound Standard Plane Detection Using a Composite Neural Network Framework. *IEEE Transactions on Cybernetics*, 47(6):1576–1586, June 2017.

[200] Geoffrey E Hinton. A practical guide to training restricted boltzmann machines. In *Neural networks: Tricks of the trade*, pages 599–619. Springer, 2012.

[201] Hugo Larochelle, Michael Mandel, Razvan Pascanu, and Yoshua Bengio. Learning algorithms for the classification restricted boltzmann machine. *Journal of Machine Learning Research*, 13(Mar):643–669, 2012.

[202] Yoshua Bengio, Li Yao, Guillaume Alain, and Pascal Vincent. Generalized denoising auto-encoders as generative models. In *Advances in Neural Information Processing Systems*, pages 899–907, 2013.

[203] Salah Rifai, Pascal Vincent, Xavier Muller, Xavier Glorot, and Yoshua Bengio. Contractive auto-encoders: Explicit invariance during feature extraction. In *Proceedings of the 28th International Conference on International Conference on Machine Learning*, pages 833–840. Omnipress, 2011.

[204] Quoc V Le, Alexandre Karpenko, Jiquan Ngiam, and Andrew Y Ng. Ica with reconstruction cost for efficient overcomplete feature learning. In *Advances in neural information processing systems*, pages 1017–1025, 2011.

[205] Geoffrey E Hinton, Alex Krizhevsky, and Sida D Wang. Transforming auto-encoders. In *International Conference on Artificial Neural Networks*, pages 44–51. Springer, 2011.

[206] Geoffrey E Hinton, Simon Osindero, and Yee-Whye Teh. A fast learning algorithm for deep belief nets. *Neural computation*, 18(7):1527–1554, 2006.

[207] Shekoofeh Azizi, Farhad Imani, Bo Zhuang, Amir Tahmasebi, Jin Tae Kwak, Sheng Xu, Nishant Uniyal, Baris Turkbey, Peter Choyke, Peter Pinto, et al. Ultrasound-based detection of prostate cancer using automatic feature selection with deep belief networks. In *International Conference on Medical Image Computing and Computer-Assisted Intervention*, pages 70–77. Springer, 2015.

[208] Jun Shi, Shichong Zhou, Xiao Liu, Qi Zhang, Minhua Lu, and Tianfu Wang. Stacked deep polynomial network based representation learning for tumor classification with small ultrasound image dataset. *Neurocomputing*, 194:87–94, 2016.

[209] Qi Zhang, Yang Xiao, Wei Dai, Jingfeng Suo, Congzhi Wang, Jun Shi, and Hairong Zheng. Deep learning based classification of breast tumors with shear-wave elastography. *Ultrasonics*, 72:150–157, 2016.

[210] Tarek M Hassan, Mohammed Elmogy, and El-Sayed Sallam. Diagnosis of focal liver diseases based on deep learning technique for ultrasound images. *Arabian Journal for Science and Engineering*, 42(8):3127–3140, 2017.

[211] Ruud JG van Sloun and Libertario Demi. Localizing b-lines in lung ultrasonography by weakly-supervised deep learning, in-vivo results. *IEEE Journal of Biomedical and Health Informatics*, 2019.

[212] `https://www.accessdata.fda.gov/cdrh_docs/pdf19/K190442.pdf`.

[213] `https://www.accessdata.fda.gov/scripts/cdrh/cfdocs/cfpma/pma.cfm?id=P150043`.

[214] `https://captionhealth.com/`.

[215] `https://www.accessdata.fda.gov/cdrh_docs/pdf19/K192388.pdf`.

[216] `https://www.accessdata.fda.gov/cdrh_docs/pdf18/K181290.pdf`.

[217] M. Brock, T. Eggert, R. J. Palisaar, F. Roghmann, K. Braun, B. Loppenberg, F. Sommerer, J. Noldus, and C. von Bodman. Multiparametric ultrasound of the prostate: adding contrast enhanced ultrasound to real-time elastography to detect histopathologically confirmed cancer. *Journal of Urology*, 189(1):93–8, 2013.

[218] P. A. Pinto, P. H. Chung, A. R. Rastinehad, A. A. Baccala, J. Kruecker, C. J. Benjamin, S. Xu, P. Yan, S. Kadoury, C. Chua, J. K. Locklin, B. Turkbey, J. H. Shih, S. P. Gates, C. Buckner, G. Bratslavsky, W. M. Linehan, N. D. Glossop, P. L. Choyke, and B. J. Wood. Magnetic resonance imaging/ultrasound fusion guided prostate biopsy improves cancer detection following transrectal ultrasound biopsy and correlates with multiparametric magnetic resonance imaging. *Journal of Urology*, 186(4):1281–5, 2011.

[219] Y. Bengio, A. Courville, and P. Vincent. Representation learning: A review and new perspectives. *IEEE Transactions on Pattern Analysis & Machine Intelligence*, 35(8):1798–1828, 2013.